Reviewer 1

In this manuscript, Pommier et al., report a set of formic acid (HCOOH) enhancement ratios with respect to carbon monoxide (CO) derived from 2008 – 2014 IASI measurements. The authors pay special attention to 7 biomass burning regions comparing their estimates with previous studies. The comparisons show reasonable agreement. In the context of recent studies reporting large underestimations in the HCOOH atmospheric budget (i.e. Stavrakou et al. 2011) the IASI dataset can help to understand a fraction of the underestimation. However for publication in ACP I suggest the paper to undergo major revisions.

The authors would like to thank reviewer 1 for his comments which help to improve our study. We have tried to clarify the points raised by the reviewer and to answer all remarks. Our responses are written in blue in this document.
Sect. 5.1 and 5.2 have been largely rewritten and are not copied in the present replies in full, thus also please read the revised manuscript.

Abstract: With the evidence provided in the text the following sentence is not fully supported "The comparison with other studies highlights a possible underestimation by 60% of emission or a secondary production of HCOOH by Siberian forest fires while the studied fire plumes originating from Southern African savanna could suggests a limited secondary production of HCOOH or a limited sink." The differences in ER between different studies, need to be explained to support such conclusion.
This is a good remark. This statement has been deleted from the abstract, we have however added theses sentences (in bold) in the conclusion:
"The underestimation by 60% over Siberia is consistent with conclusions given in R'Honi et al. (2013). **The calculation of the $ER_{(HCOOH/CO)}$ by biome shows that Siberian plumes are related to the burning of six different vegetation classes. The underestimation reported is thus difficult to confirm without the use of a chemical transport model**."

We have also written in Section 5.2:
"These hypotheses in biased emissions and/or secondary production need, however, to be verified with modeling studies."

Section 4.2: Figure 2 provides a qualitative analysis. HCOOH and CO concentrations apparently track MODIS fire counts. Working out correlations coefficients for CO, HCOOH and fire counts separately will help to address the origin of the air masses and what is the influence of the fire activity on them.
The monthly means does not present a clear correlation as illustrated in Fig. 2 and explained by the sentence in the ACPD manuscript in Section 4.2 (lines 150-152) "It is also worth noting that these variations in the total columns do not depend on the intensity of the fires as shown by Fig. 2 and by the scatterplots with the values characterizing each fire as described below (not shown)."

The impact of the fire activity (FRP) was, however, studied. We did not find correlations between the intensity of each fire and the amount of CO or HCOOH (see Table below for each region) despite that the enhancements in the IASI-derived columns can confidently be attributed to fires. We have decided not to show these results in the manuscript.

region	Criteria: time=[0 5h], r=50km	Criteria: time=[0 5h], r=50km, ws<1.44 m/s
NAF	r (FRP-HCOOH)=0.02 r (FRP-CO)=0.1	r (FRP-HCOOH)=-0.09 r (FRP-CO)=0.13
AMA	r (FRP-HCOOH)=0.03 r (FRP-CO)=0.03	r (FRP-HCOOH)=0.01 r (FRP-CO)=-0.04
AUS	r (FRP-HCOOH)=0.1 r (FRP-CO)=0.08	r (FRP-HCOOH)=0.01 r (FRP-CO)=-0.08
SIB	r (FRP-HCOOH)=0.11 r (FRP-CO)=0.08	r (FRP-HCOOH)=0.2 r (FRP-CO)=0.21
SAF	r (FRP-HCOOH)=0.04 r (FRP-CO)=0.09	r (FRP-HCOOH)=0.05 r (FRP-CO)=0
SEA	r (FRP-CO)=0.13 r (FRP-CO)=0.11	r (FRP-HCOOH)=0.24 r (FRP-CO)=0.18
IND	r (FRP-HCOOH)=0.04 r (FRP-CO)=0.02	r (FRP-HCOOH)=0.08 r (FRP-CO)=0.1

Sections 4.2 and 4.3: The authors try to isolate IASI retrievals influenced by biomass burning using MODIS and ECMWF data. While the definition of the biomass burning regions based in MODIS fire counts is clear, it is not clear to me how co-located IASI data are selected. Quoting the text: "To do so, we co-located the IASI data at 50 km around each MODIS pixel and between 0 and 5h for each detected fire, so that each MODIS pixel is associated with a value of HCOOH and CO total column from IASI".
Further clarification is needed. All these questions are not answered in the description given in the text. For a MODIS pixel is it possible to have more than one IASI retrieval within 50 km? If so, the associated value for that MODIS fire is the average? MODIS has a resolution of 1km by 1km, a given retrieval can be accounted several times due to adjacent MODIS fire pixels. What does it mean 0 and 5 h for each detected fire? 5 hours ahead and 5 hours behind? With MODIS overpass times at 10:30am and 13:30am the night time IASI measurements 9:30pm will always be excluded. What is the influence of modifying the 50 km and 5 hour threshold in the results?

The criteria used correspond to a radius of 50 km around each MODIS hotspot and the time = [0 5h]. Then all the IASI data collocated around each MODIS hotspot were averaged.
To clarify this point we have changed the sentence in the manuscript to:
"To do so, we co-located the IASI data at 50 km around each MODIS pixel and between 0 and 5h from the time registered by MODIS for each detected fire, so that each MODIS pixel is associated with a mean value of HCOOH and CO total columns from IASI".

The idea was to get a sufficient number of hotspots with a high correlation coefficient in order to be confident in the value of the slope $\partial[HCOOH]/\partial[CO]$.
We have chosen to use as temporal criterion +5 hours instead of ±5 hours in order to avoid selecting IASI data before the starting time of a fire. Different criteria on the time difference and the spatial mismatch have been tested in addition to those used in the paper. They are summarized in the Table below but are not shown in the manuscript:

Tab. Correlation coefficients between the HCOOH total columns and the CO total columns measured by IASI for the period between 2008 and 2014 over the seven studied regions, before the use of the wind speed criterion. The results from the criteria, h=[0 5h] and r=50km used in the paper are written in red.

	AMA	AUS	IND	SEA	SAF	NAF	SIB
Criteria used in the paper	0.78 (13342)	0.63 (1525)	0.53 (1641)	0.84 (1865)	0.78 (12227)	0.58 (21139)	0.65 (22353)
h=[0 5h] r=10km	0.72 (1510)	0.49 (114)	0.64 (184)	0.78 (312)	0.69 (1965)	0.42 (2752)	0.39 (2426)
h=[0 10h] r=10km	0.63 (3624)	0.48 (1376)	0.53 (1941)	0.7 (10897)	0.69 (12211)	0.49 (5708)	0.45 (6342)
h=[0 10 h] r=50km	0.73 (32463)	0.61 (12414)	0.47 (20090)	0.74 (87378)	0.72 (124784)	0.6 (58273)	0.66 (46081)
h=[-5h +5h] r=50 km	0.79 (253188)	0.74 (33303)	0.55 (42924)	0.82 (123243)	0.81 (504733)	0.53 (439994)	0.61 (78570)

Concerning the MODIS overpass, it was an error in the text. The correct sentence and overpasses are:
"The Terra and Aqua satellites equatorial overpass times are ~10:30 (am and pm) and ~01:30 (am and pm) local time, respectively."

Surface ECMWF winds definitely increase the confidence of using only biomass burning affected IASI retrievals. However, the sensitivity of the IASI retrievals is highest between 1km and 6km. The authors should address the uncertainties introduced in the calculations due to transport vs. lofting of the air masses and influence of non-pyrogenic air masses in the IASI retrievals. This is particularly relevant for regions other than Equatorial Africa and South Africa were biomass burning signal is superimposed with other sources (Chaliyakunnel et al., 2016).

The impact of the air masses on the IASI CO and HCOOH retrievals represents a specific study which should be done but it is beyond the scope of this paper, even if it is a relevant question. However, to answer this question, we have analyzed the vertical velocity at 1000hPa provided by ECMWF and the wind speed at three levels: 825, 650 and 450 hPa. These fields have the same resolution of the data used in the paper, i.e. 0.125° × .0.125° and a 6h time step. We have checked their impact on our scatterplots as done with the surface wind speed in the manuscript.

The question about the lofting of the air masses can be studied with the vertical velocity. We have plotted the distribution over the seven regions as in figure 3 of the paper and presented hereafter:

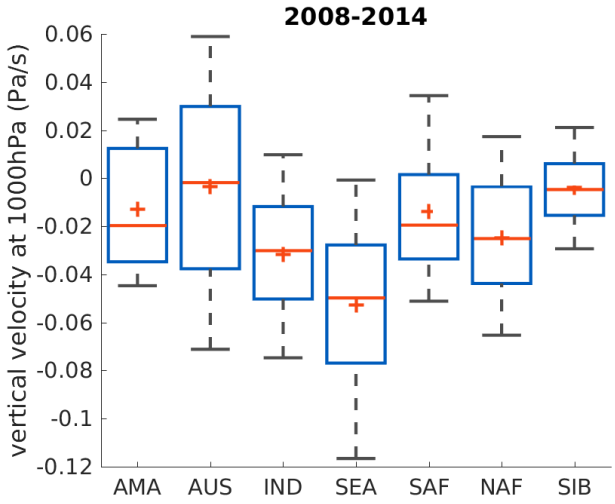

Fig. 1. Box and whisker plots showing mean (red central cross), median (red central line), and 25th and 75th percentile (blue box edges) of vertical velocity at 1000 hPa for each MODIS hotspot over the studied regions (AMA=Amazonia, AUS=Australia, IND = India, SEA = Southern East Asia, NAF= Northern Africa, SAF= Southern Africa, SIB= Siberia).

Since pressure decreases with height, negative values of the vertical velocity indicate rising motion in the atmosphere, and positive values indicate sinking air.
As shown by this figure 1, no clear relationship between the vertical velocity and the correlation found over the regions studied in our work is found. India showing a low correlation coefficient as presented in Tab. 1, does not show a particular difference with other regions. For example, SAF having a lower mean velocity and SEA having a higher mean velocity than IND, have a higher correlation coefficient than IND.
We can conclude that the vertical injection ("lofting of the air masses") has a negligible impact on our scatterplots.
It however suggests a higher rising motion of the air masses over IND and SEA as already stated in Sect. 5.2. We have decided to add this sentence (in bold):
"…this may suggests that the plumes studied over the 7-yr period correspond to fresh plumes where the chemistry or the physical sink is small. **This is further supported by the fact that among the seven regions, IND and SEA have larger vertical velocity means close to the surface indicating a larger rising motion of the air masses (not shown)**."

In order to estimate the impact of the long-range transport on our correlation coefficients, a similar methodology has been used with the wind at different pressure levels.
We chose 450, 650 and 825 hPa, corresponding approximately to 5.7, 3.1 and 1.4 km and the results are presented in Fig. 2 hereafter. These levels are within the range of vertical sensitivity of the IASI HCOOH retrieval, i.e. between 1 and 6 km. The regions showing the lowest correlation coefficient (Tab.1 in the manuscript) do not match with a high or low wind speed. It is however shown that a high mean and median wind speed are noticed over IND and SEA.
These distributions do not allow the identification of a clear influence of the long-range transport in our scatterplots.

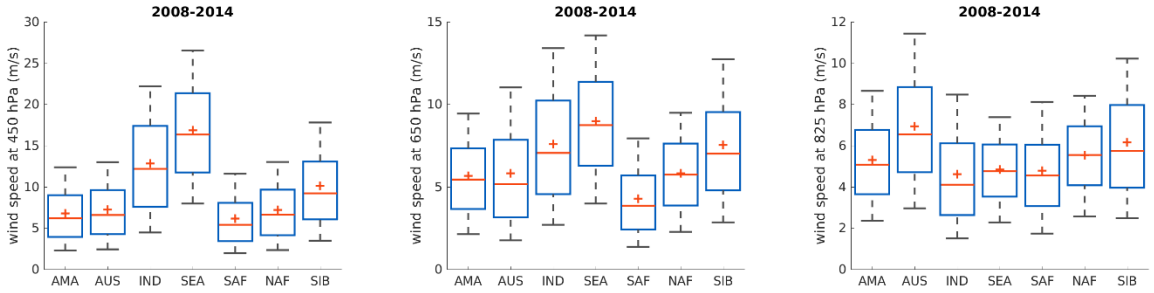

Fig. 2. Box and whisker plots showing mean (red central cross), median (red central line), and 25th and 75th percentile (blue box edges) of wind speed at 450, 650 and 825hPa for each MODIS hotspot over the studied regions (AMA=Amazonia, AUS=Australia, IND = India, SEA = Southern East Asia, NAF= Northern Africa, SAF= Southern Africa, SIB= Siberia).

We have added these sentences in Sect. 4.3:
"It is also noteworthy that the IND and SEA regions are both characterized by higher wind speed at higher altitudes, i.e. for the pressure levels 650 and 450 hPa (not shown). This shows that the wind speed at higher altitudes has a lower influence on our correlations than the surface wind."

Table 1 and 2 can be combined in one single table.
It is a good suggestion. Both tables are now merged as below:

Table 1 Upper row: Correlation coefficients between the HCOOH total columns and the CO total columns measured by IASI for the period between 2008 and 2014 over the seven studied regions. Lower row: As upper row but with only MODIS fire hotspot having a surface wind speed lower than 1.44 m/s. Each IASI data is selected in an area of 50 km around the MODIS fire hotspot and up to 5h after the time recorded for each fire. The number of fires characterized by HCOOH and CO total columns is given in parenthesis.

	AMA	AUS	IND	SEA	SAF	NAF	SIB
r	0.78 (13342)	0.63 (1525)	0.53 (1641)	0.84 (1865)	0.78 (12227)	0.58 (21139)	0.65 (22353)
	0.79 (4580)	0.65 (93)	0.65 (340)	0.86 (528)	0.80 (895)	0.53 (1095)	0.72 (2097)

Sections 5.1 & 5.2: What is the reason for the exception in Siberia where using only columns with a thermal contrast larger than 10K changed the ER from 6.5 mol/mol to 4.4 mol/mol.
More explanations are now given and the new paragraph is (the modifications are highlighted in bold):
"Nevertheless, in order to investigate the possible impact of the overestimation in the lower columns **and the underestimation in the higher columns** on the calculated ratios, a test was performed, by using only HCOOH columns with a thermal contrast larger than 10K. Indeed, the increase in the thermal contrast (i.e. the temperature difference between the surface and the first layer in the retrieved profile) leads to **reducing** the detection limit as shown in Pommier al. (2016**). This enhancement of the detection level helps to minimize the bias in the retrieved total columns as explained in Crevoisier et al. (2014). For the analysis performed here, similar slopes and correlation coefficients were generally calculated**, suggesting a negligible effect of this parameter on the biases. The only exception is an increase in $ER_{(HCOOH/CO)}$ over **Siberia ($6.5\times10^{-3} \pm 0.19\times10^{-3}$ mol/mol when using only IASI**

measurements with TC above 10K against 4.4×10^{-3} mol/mol ± 0.09×10^{-3} in Table 2). It is worth noting that only 48% of the selected scenes remain over Siberia when applying this filter on thermal contrast (60% for SEA, 77% for AMA, 80% for SAF, 83% for AUS and NAF, and 89% for IND). This implies that the statistics on the fire emissions in the higher latitudes of Siberia is dominated by measurements with a low thermal contrast and thus with HCOOH total columns with higher uncertainties. However, the limited changes in slopes and correlation coefficients give us confidence that the results presented in Table 2 are **representative**."

Ground based FTIR, IASI, ACE-FTS, TES, and airborne FTIR are sensitive to different altitudes. The good agreement over Southern Africa can be linked with the distinctive burning season and air masses not containing other origins. That can explain why when ACE-FTS samples air masses that have travelled across the Atlantic Ocean (Risland et al., 2006) the ER are significant. Therefore, to extract quantitative conclusions from the comparison exercise, it is necessary to have information about the origin of the air masses and the type of fuel burned. The authors can address these two issues using back trajectory model, for example Hysplit, and MODIS land surface type. As the manuscript stands now the discussion is mostly speculative.
It is a good remark from the reviewer.

As there are 9628 MODIS hotspots studied in this paper, it is difficult to calculate backward trajectories for each hotspot, especially as different altitude ranges need to be tested since the vertical sensitivity of IASI (CO & HCOOH) is located in the free troposphere.
In order to investigate this, a few tests were done to show the distinct origins of the air masses at different locations, periods of the year and altitudes of the plume. Specifically 5 hotspots have been chosen randomly for each region and 3 different altitudes have been used: 500 m (thus close to the surface), 2000 m and 5000 m (representing the free troposphere). In total, this represents 105 trajectories.
These trajectories show that the air masses initialized at 500 and 2000m are mainly influencing by air masses close to the surface, confirming an origin near the source of our IASI fire-affected columns. It also shows the difficulty to estimate the origin of the air masses without an accurate knowledge of the altitude of the plumes.
These trajectories were plotted through the HYSPLIT online service:

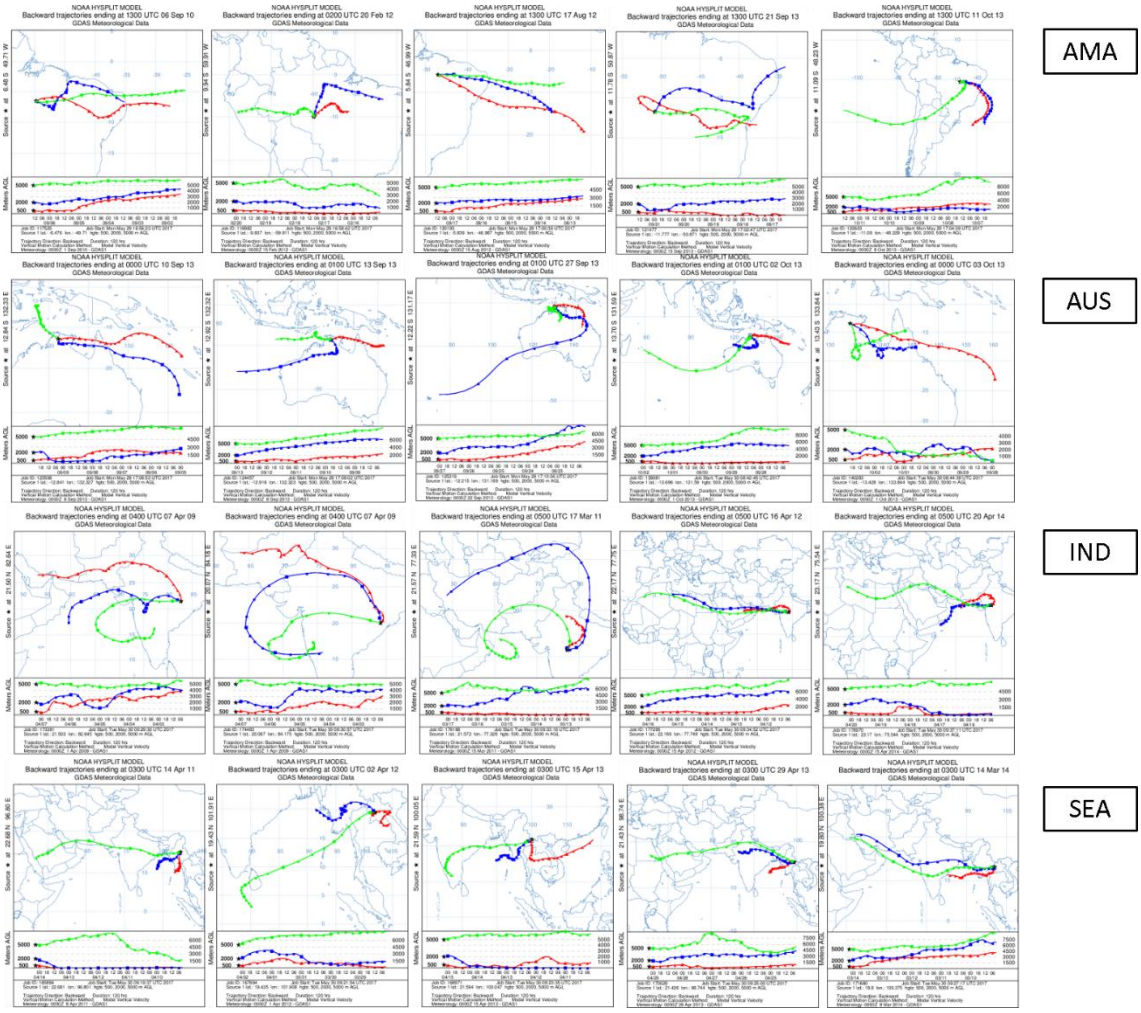

Fig 3. 5-day backward trajectories from HYSPLIT online service calculated at 3 altitudes: 500 m (red), 2000 m (blue) and 5000 m (green), for 5 hotspots chosen randomly over the 7 regions studied in the paper. The parameters characterizing each MODIS hotpots are summarized in the following table. The meteorological fields are from GDAS at 1°×1° horizontal resolution.

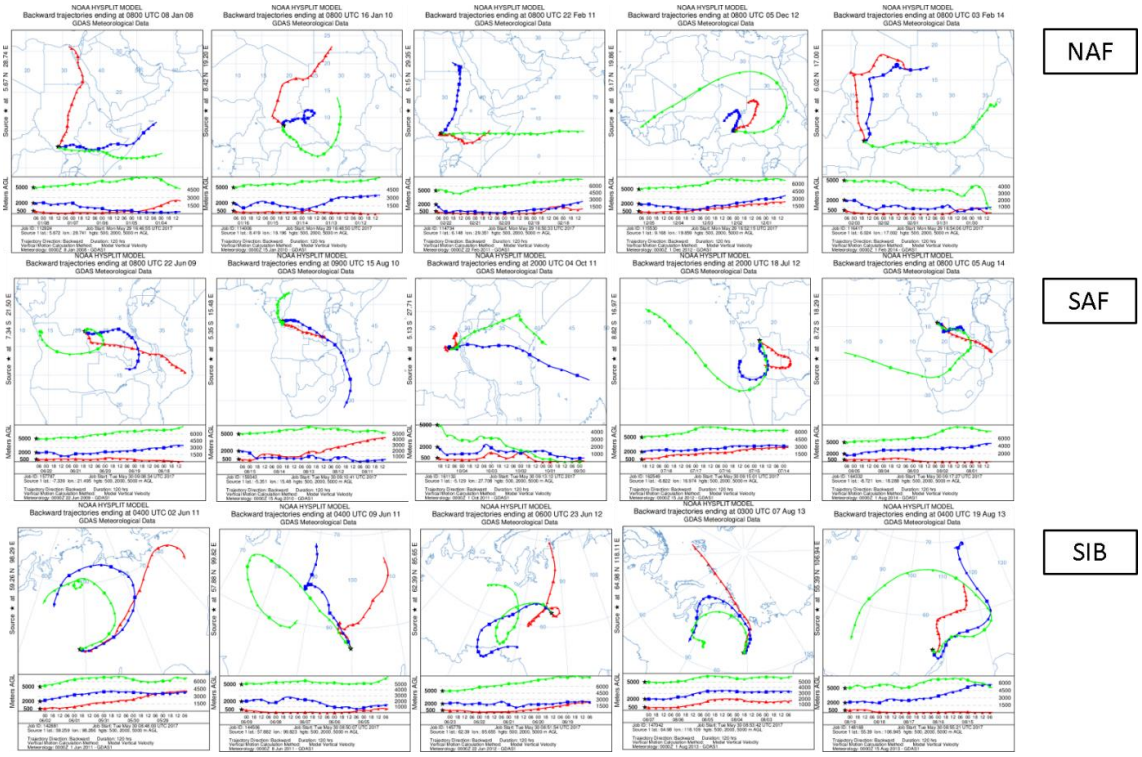

Fig 3. Continue

Tab. Characteristic of each MODIS hotspot used for the trajectories plotted in the previous figure. The dates, the time recorded by the instrument and the coordinates for each hotspot are written.

AMA
20100906 / hour (UTC)=13 / lat=-6.476 - lon=-49.71
20120220 / hour (UTC)=2 / lat=-9.937 - lon=-59.911
20120817 / hour (UTC)=13 / lat=-5.839 - lon=-46.987
20130921 / hour (UTC)=13 / lat=-11.777 - lon=-50.871
20131011 / hour (UTC)=13 / lat=-11.09 - lon=-48.229
AUS
20130910 / hour (UTC)=0 / lat=-12.841 - lon=132.327
20130913 / hour (UTC)=1 / lat=-12.916 - lon=132.323
20130927 / hour (UTC)=1 / lat=-12.215 - lon=131.169
20131002 / hour (UTC)=1 / lat=-13.696 - lon=131.59
20131003 / hour (UTC)=0 / lat=-13.428 - lon=133.844
IND
20090407 / hour (UTC)=4 / lat=21.503 - lon=82.645
20090407 / hour (UTC)=4 / lat=20.067 - lon=84.175
20110317 / hour (UTC)=5 / lat=21.572 - lon=77.328
20120416 / hour (UTC)=5 / lat=22.166 - lon=77.749
20140420 / hour (UTC)=5 / lat=23.17 - lon=75.544
SEA
20110414 / hour (UTC)=3 / lat=22.681 - lon=96.801
20120402 / hour (UTC)=3 / lat=19.435 - lon=101.908
20130315 / hour (UTC)=3 / lat=21.594 - lon=100.047
20130329 / hour (UTC)=3 / lat=21.426 - lon=98.744
20140314 / hour (UTC)=3 / lat=19.8 - lon=100.375

NAF
20080108 / hour (UTC)=8 / lat=5.672 - lon=28.741
20100116 / hour (UTC)=8 / lat=8.419 - lon=19.196
20110222 / hour (UTC)=8 / lat=6.148 - lon=29.351
20121205 / hour (UTC)=8 / lat=9.168 - lon=19.859
20140203 / hour (UTC)=8 / lat=6.024 - lon=17.002
SAF
20090622 / hour (UTC)=8 / lat=-7.339 - lon=21.495
20100815 / hour (UTC)=9 / lat=-5.351 - lon=15.48
20111004 / hour (UTC)=20 / lat=-5.129 - lon=27.708
20120718 / hour (UTC)=20 / lat=-8.822 - lon=16.974
20140805 / hour (UTC)=8 / lat=-8.721 - lon=18.288
SIB
20110602 / hour (UTC)=4 / lat=59.259 - lon=98.286
20110609 / hour (UTC)=4 / lat=57.882 - lon=99.823
20120623 / hour (UTC)=6 / lat=62.39 - lon=85.655
20130807 / hour (UTC)=3 / lat=64.98 - lon=118.109
20130819 / hour (UTC)=4 / lat=55.39 - lon=106.945

To reply to this point, we have added the following sentences (in bold) in the text:
"A few backward trajectories (along 5 days, not shown) have been calculated for our hotspots with the online version of the HYSPLIT atmospheric transport and dispersion modeling system (Rolph, 2017). These trajectories, initialized at different altitudes, confirm a main origin close to the surface of our IASI fire-affected columns. It is however impossible to properly compare the origin of the air masses with previous studies as our studied period (2008-2014) or our studied fires do not necessarily match with plumes described in other publications. It is also difficult to estimate the age of our studied air masses by gathering the plumes during a 7-yr period and without an accurate knowledge of the altitude of the plumes."

And:

"One possible explanation is the multi-origin of the plumes studied by Rinsland et al. (2006), since, based on their backward trajectories, their plumes could be influenced by biomass burning originating from Southern Africa and/or from Southern America. **The travel during the few days across the Atlantic Ocean may explain the change in their $ER_{(HCOOH/CO)}$."**

With the corresponding reference:
Rolph, G.D.: Real-time Environmental Applications and Display sYstem (READY) Website (http://www.ready.noaa.gov). NOAA Air Resources Laboratory, College Park, MD, 2017.

About the type of fuel burned, thanks to the reviewer, we have discovered that such information was available from the MODIS products.
Now, in Section 3. MODIS we have added this paragraph:
"To characterize each MODIS hotspot by the type of fuel burned, the Global Mosaics of the standard MODIS land cover type data product (MCD12Q1) in the IGBP Land Cover Type Classification (Friedl et al., 2010; Channan et al., 2014) with a 0.5° × 0.5° horizontal resolution has also been used (http://glcf.umd.edu/data/lc/). As the annual variability in this product is

limited (not shown) and since the period available (from 2001 to 2012) does not fully match the period of the IASI mission, only the data for 2012 have been used. Whitburn et al. (2017) have also used this MCD12Q1 product to determine their IASI-derived NH_3 enhancement ratios by vegetation types."

With the corresponding references:

Channan, S., Collins, K., and Emanuel, W. R., Global mosaics of the standard MODIS land cover type data. University of Maryland and the Pacific Northwest National Laboratory, College Park, Maryland, USA, 2014.

and

Friedl, M. A., Sulla-Menashe, D., Tan, B., Schneider, A., Ramankutty, N., Sibley, A. and Huang, X., MODIS Collection 5 global land cover: Algorithm refinements and characterization of new datasets, 2001-2012, Collection 5.1 IGBP Land Cover, Remote Sensing of Environment, 114 , 168–182, doi:10.1016/j.rse.2009.08.016, 2010.

and

Whitburn, S., Van Damme, M., Clarisse, L., Hurtmans, D., Clerbaux, C., and Coheur, P.-F.: IASI-derived NH3 enhancement ratios relative to CO for the tropical biomass burning regions, Atmos. Chem. Phys. Discuss., https://doi.org/10.5194/acp-2017-331, in review, 2017.

We have also added this sentence in Section 4.2:

"The classification of the vegetation from the MODIS product has also been used for a detailed analysis of the enhancement ratios for these regions (Fig. 1)."

And Fig. 1 has been modified as below:

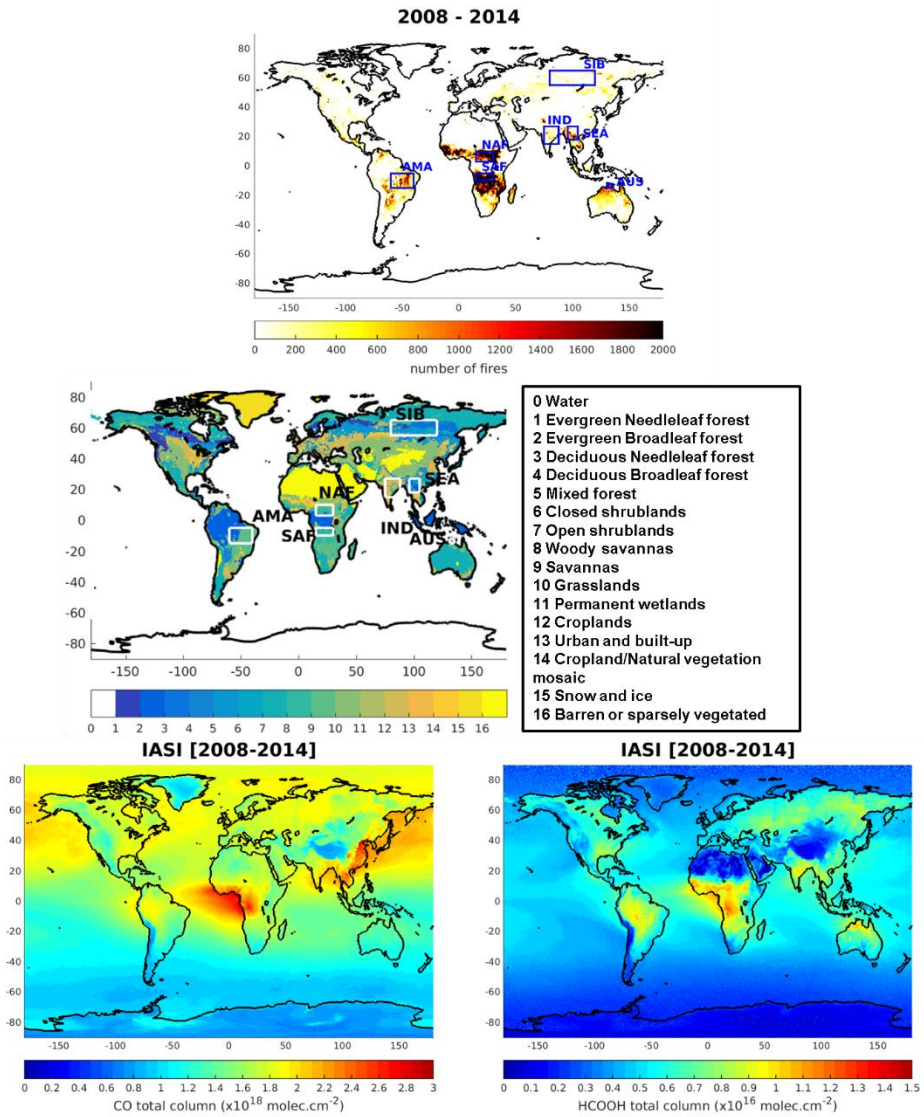

Figure 1: Top: Number of MODIS fire hotspots with a confidence percentage higher or equal to 80%, averaged on a 0.5°×0.5° grid, for the period between 2008 and 2014. The blue boxes are the regions studied in this work. Middle: Classification of the land cover type from MODIS on the same grid and highlighting the studied regions in white. Each number corresponds to the type of vegetation. Only the data between 64°S and 84°N are available. Bottom: The IASI CO total column distribution (left) and the IASI HCOOH total column distribution (right), averaged between 2008 and 2014 and on the same grid.

Section 5.2 was also rewritten and now named "5.2. Analysis based on the type of vegetation" since ER (HCOOH/CO) by type of vegetation were also added in Table 3 as below:

Table 3. Enhancement ratio of HCOOH relative to CO (mol/mol) with its standard deviation and enhancement ratio of HCOOH relative to CO (mol/mol) by biome with its standard deviation calculated in this work. For each enhancement ratio by biome, the correlation coefficient and the number of MODIS hotspots are provided. The enhancement ratios are compared to emission ratios calculated from emission factors given in the literature for the seven studied regions. For the calculation of these emission ratios, the emission factors of CO for the corresponding fuel type given in Akagi et al. (2011) are used. Emission ratios of HCOOH relative to CO (mol/mol) calculated from the emission factors of HCOOH given in Akagi et al. (2011) for the corresponding fuel type are also provided.

Region	**Enhancement Ratio to CO (mol/mol) – this work**	**Enhancement Ratio to CO (mol/mol)[1] by biome[2] – this work**	Emission Ratio to CO (mol/mol) calculated from EF_{HCOOH} given in literature and using EF_{CO} from Akagi et al. (2011)	Instrument used
AMA	**$7.3\times10^{-3} \pm 0.08\times10^{-3}$**	**$6.3\times10^{-3} \pm 0.22\times10^{-3}$ (Evergreen Broadleaf forest, r=0.81, n = 454)** **$3.0\times10^{-3} \pm 0.81\times10^{-3}$ (Open shrubland, r=0.91, n = 5)** **$7.0\times10^{-3} \pm 2.47\times10^{-3}$ (Woody savanna, r=0.63, n = 14)** **$7.6\times10^{-3} \pm 0.09\times10^{-3}$ (Savanna, r=0.79, n = 3909)** **$8.4\times10^{-3} \pm 0.39\times10^{-3}$ (Grassland, r=0.88, n = 143)** **$4.6\times10^{-3} \pm 0.35\times10^{-3}$ (Cropland, r=0.88, n = 54)**	1.8×10^{-3} – Tropical forest (Yokelson et al., 2007 ; 2008)[3] 2.7×10^{-3} – Savanna (Yokelson et al., 2007 ; 2008)[3] 2.0×10^{-3} – Savanna (Akagi et al., 2011) 5.2×10^{-3} – Tropical forest (Akagi et al., 2011)	Airborne FTIR (Yokelson et al., 2007) ; laboratory (Yokelson et al., 2008) catalogue
AUS	**$11.1\times10^{-3} \pm 1.37\times10^{-3}$**	**$5.7\times10^{-3} \pm 2.55\times10^{-3}$ (Woody savanna, r=0.6, n = 11)** **$11.2\times10^{-3} \pm 1.49\times10^{-3}$ (Savanna, r=0.65, n = 80)**	2.0×10^{-3} – Savanna (Akagi et al., 2011)	catalogue
IND	**$6.8\times10^{-3} \pm 0.44\times10^{-3}$**	**$6.6\times10^{-3} \pm 0.77\times10^{-3}$ (Woody savanna, r=0.65, n = 103)** **$6.2\times10^{-3} \pm 0.62\times10^{-3}$ (Cropland, r=0.58, n = 198)** **$8.8\times10^{-3} \pm 1.19\times10^{-3}$ (Cropland/Natural vegetation mosaic, r=0.85, n =23)**	2.0×10^{-3} – Savanna (Akagi et al., 2011) 2.7×10^{-3} – Extratropical forest (Akagi et al., 2011) 6.0×10^{-3} – Cropland (Akagi et al., 2011)	catalogue
SEA	**$5.8\times10^{-3} \pm 0.15\times10^{-3}$**	**$5.6\times10^{-3} \pm 0.20\times10^{-3}$ (Evergreen Broadleaf forest, r=0.83, n = 334)**	2.0×10^{-3} – Savanna (Akagi et al., 2011) 2.7×10^{-3} – Extratropical forest (Akagi et al., 2011) 6.0×10^{-3} – Cropland (Akagi et al., 2011)	catalogue

		$6.3\times10^{-3} \pm 0.66\times10^{-3}$ (Mixed forest, r=0.76, n = 70) **$6.2\times10^{-3} \pm 0.38\times10^{-3}$ (Woody savanna, r=0.86, n = 99)** **$7.1\times10^{-3} \pm 0.99\times10^{-3}$ (Cropland/Natural vegetation mosaic, r=0.84, n =23)**		
NAF	**$4.0\times10^{-3} \pm 0.19\times10^{-3}$**	**$3.4\times10^{-3} \pm 0.63\times10^{-3}$ (Evergreen Broadleaf forest, r=0.52, n = 78)** **$3.3\times10^{-3} \pm 0.28\times10^{-3}$ (Woody savanna, r=0.44, n = 569)** **$4.4\times10^{-3} \pm 0.29\times10^{-3}$ (Savanna, r=0.59, n = 441)** **$22.6\times10^{-3} \pm 11.06\times10^{-3}$ (Cropland/Natural vegetation mosaic, r=0.67, n = 7)**	2.0×10^{-3} – Savanna (Akagi et al., 2011)	catalogue
SAF	**$5.0\times10^{-3} \pm 0.13\times10^{-3}$**	**all hotspots are woody savanna**	3.3×10^{-3} – Tropical forest (Sinha et al., 2004)[4] 4.8×10^{-3} – Savanna (Sinha et al., 2004)[4] 4.1×10^{-3} – Tropical forest (Yokelson et al., 2003) 6.0×10^{-3} – Savanna (Yokelson et al., 2003) 13×10^{-3} – Tropical forest (Rinsland et al., 2006) 19.2×10^{-3} – Savanna (Rinsland et al., 2006) 2.0×10^{-3} – Savanna (Akagi et al., 2011) 5.2×10^{-3} – Tropical forest (Akagi et al., 2011)	Airborne FTIR Airborne FTIR ACE-FTS catalogue
SIB	**$4.4\times10^{-3} \pm 0.09\times10^{-3}$**	**$4.0\times10^{-3} \pm 0.31\times10^{-3}$ (Evergreen Needleaf forest, r=0.63, n = 245)** **$3.6\times10^{-3} \pm 0.16\times10^{-3}$ (Deciduous Needleaf forest, r=0.66, n = 659)** **$3.4\times10^{-3} \pm 0.18\times10^{-3}$ (Mixed forest, r=0.57, n = 759)**	2.7×10^{-3} – Boreal forest (Akagi et al., 2011)	catalogue

	$6.6\times10^{-3} \pm 0.48\times10^{-3}$ (Open shrubland, r=0.76, n = 143) **$6.0\times10^{-3} \pm 0.41\times10^{-3}$ (Woody savanna, r=0.76, n = 155)** **$3.8\times10^{-3} \pm 0.65\times10^{-3}$ (Permanent wetland, r=0.6, n = 63)**

[1] Only the enhancement ratio to CO calculated from a scatterplot with a correlation coefficient higher than 0.4 are reported.
[2] The type of vegetation is defined by the land cover type data product (MCD12Q1).
[3] The EF_{HCOOH} were corrected based on the comment from Yokelson et al. (2013) (EF_{HCOOH} used: 0.281 for Yokelson et al. (2007); 0.2767 for Yokelson et al. (2008)).
[4] The mean of both EF_{HCOOH} values provided in Sinha et al. (2004) were used for our $EmR_{HCOOH/CO}$ calculation

We have added these sentences at the end of the Section 5.2:
"In addition to the $EmR_{(HCOOH/CO)}$ calculated from the EF_{HCOOH} given in the literature, a classification for our $ER_{(HCOOH/CO)}$ has also been done, based on the data from the MCD12Q1 product. As each hotspot is associated with a land cover value defined by the MCD12Q1 product, enhancement ratios by biome have been calculated. The limitations of this dataset are its coarse resolution (0.5° × 0.5°) and the lack of seasonal variation. It gives however a supplementary information on the type of fuel burned identified by MODIS. The corresponding $ER_{(HCOOH/CO)}$ are provided in Table 3. Only the values calculated from a scatterplot with a correlation coefficient higher than 0.4 are reported."

And

"In general, the $ER_{(HCOOH/CO)}$ calculated for a specific biome varies with the regions. This shows that the type of vegetation is not the only factor influencing the $ER_{(HCOOH/CO)}$. The ongoing chemistry within a plume is important and the age of the air masses impact the level of HCOOH and CO in the plumes."

We have also added these sentences in the abstract:
"An additional classification of the enhancement ratios by type of fuel burned is also provided, showing a diverse origin of the plumes sampled by IASI, especially over Amazonia and Siberia. The variability in the enhancement ratios by biome over the different regions show that the levels of HCOOH and CO do not only depend on the fuel types."
And in the conclusion:
"Finally, the estimation of the $ER_{(HCOOH/CO)}$ calculated by the type of vegetation burned, as referenced in the MODIS product, varies with the regions. This shows that other parameters than the type of fuel burned also influence the $ER_{(HCOOH/CO)}$."

Conclusions: As with the abstract "Fires over Australia and over Siberia are probably underestimated in terms of direct emission or secondary production of HCOOH. The analysis over Australia is however delicate as our ER (HCOOH/CO) approximately corresponds to the mean of the values reported in Paton- Walsh et al. (2005) and in Chaliyakunnel et al. (2016); and is also 450% higher than the E m R (HCOOH/CO) derived from Akagi et al. (2011). The underestimation by 60% over Siberia is consistent with conclusions given in R'Honi et al., (2103)." a more detailed analysis is needed to link differences in ER with direct emission and secondary production.

It is correct. See our responses to your first comment (abstract).

Finally, IASI is also capable of measuring HCN a useful biomass burning tracer. It will be useful if the authors discussed the possibility of using it in future analysis.
It is a good remark. This sentence has been modified (in bold) in the conclusion:
"This IASI data set may also be used in the future to study a single plume at different times **to inform on the loss during transport. Further insight into the transport and chemistry may be gained by using IASI's capability to measure several fire species simultaneously, such as HCN or C_2H_2 (e.g. Duflot et al., 2015**)."

The corresponding reference has also been added:
Duflot, V., Wespes, C., Clarisse, L., Hurtmans, D., Ngadi, Y., Jones, N., Paton-Walsh, C., Hadji-Lazaro, J., Vigouroux, C., De Mazière, M., Metzger, J.-M., Mahieu, E., Servais, C., Hase, F., Schneider, M., Clerbaux, C., and Coheur, P.-F.: Acetylene (C_2H_2) and hydrogen cyanide (HCN) from IASI satellite observations: global distributions, validation, and comparison with model, Atmos. Chem. Phys., 15, 10509-10527, doi:10.5194/acp-15-10509-2015, 2015.

Technical comments:
A revision of the English used could improve the transparency and clarity of the paper, particularly in the introduction.
It has been done.

Line 68, please include reference to Razavi et al., 2011 (first HCOOH retrievals from IASI).
The reference has been added.

Line 71, please include Gonzalez Abad et al., 2009 in ACE-FTS papers.
The reference has been added.

Line 98, please include citation about IASI CO2 retrievals.
This following reference has been added:
Crevoisier, C., Chédin, A., Matsueda, H., Machida, T., Armante, R., and Scott, N. A.: First year of upper tropospheric integrated content of CO_2 from IASI hyperspectral infrared observations, Atmos. Chem. Phys., 9, 4797-4810, doi:10.5194/acp-9-4797-2009, 2009.

Line 118, correct typo (Pommier et al., 2016).
Done

Line 141, actives to become active.
Changed.

Line 206, should read "Both biases are however" instead of "Both biases is howeve"
It reads now:
"The effects of both biases are, however, limited since most of HCOOH…"

Line 282, please specify which other studies.
This information is now available (in bold) in the following sentence:
"For the other regions, in addition to the values from Akagi et al. (2011), emission ratios were similarly calculated from emission factors given in other studies **(listed in Table 3)**."

Figure 2, include units in plots.

Figure 4, please include units in plots.
Figs 2 and 4 now include units, as hereafter:

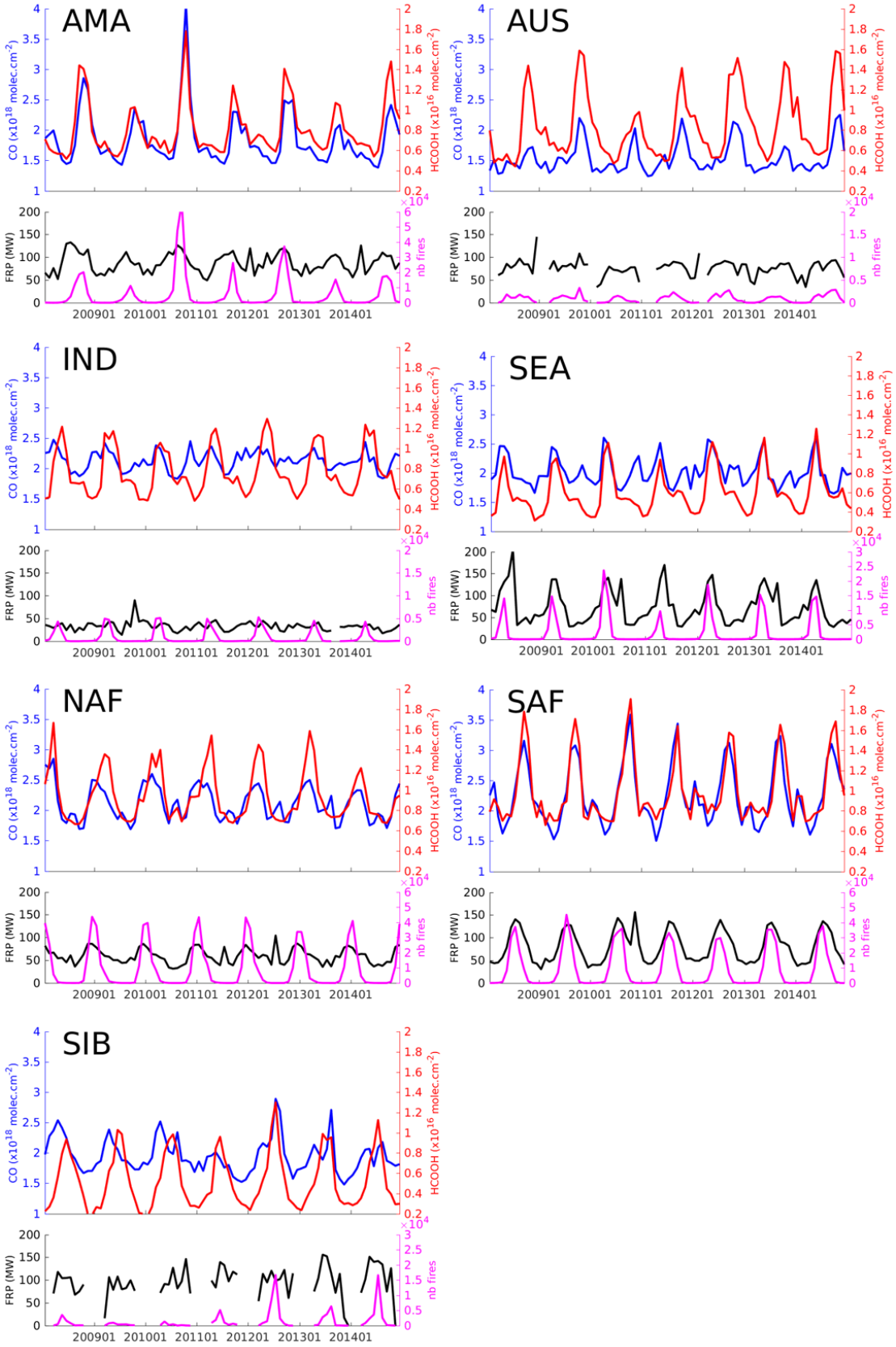

Figure 2: Time-series from 2008 to 2014 of the monthly means of IASI CO (blue) and HCOOH (red) total columns in 10^{18} molec/cm^2 and in 10^{16} molec/cm^2, respectively, FRP (black) in MegaWatts and the number of fires (magenta) from

MODIS over the seven regions (AMA=Amazonia, AUS=Australia, IND = India, SEA = Southern East Asia, NAF= Northern Africa, SAF= Southern Africa, SIB= Siberia).

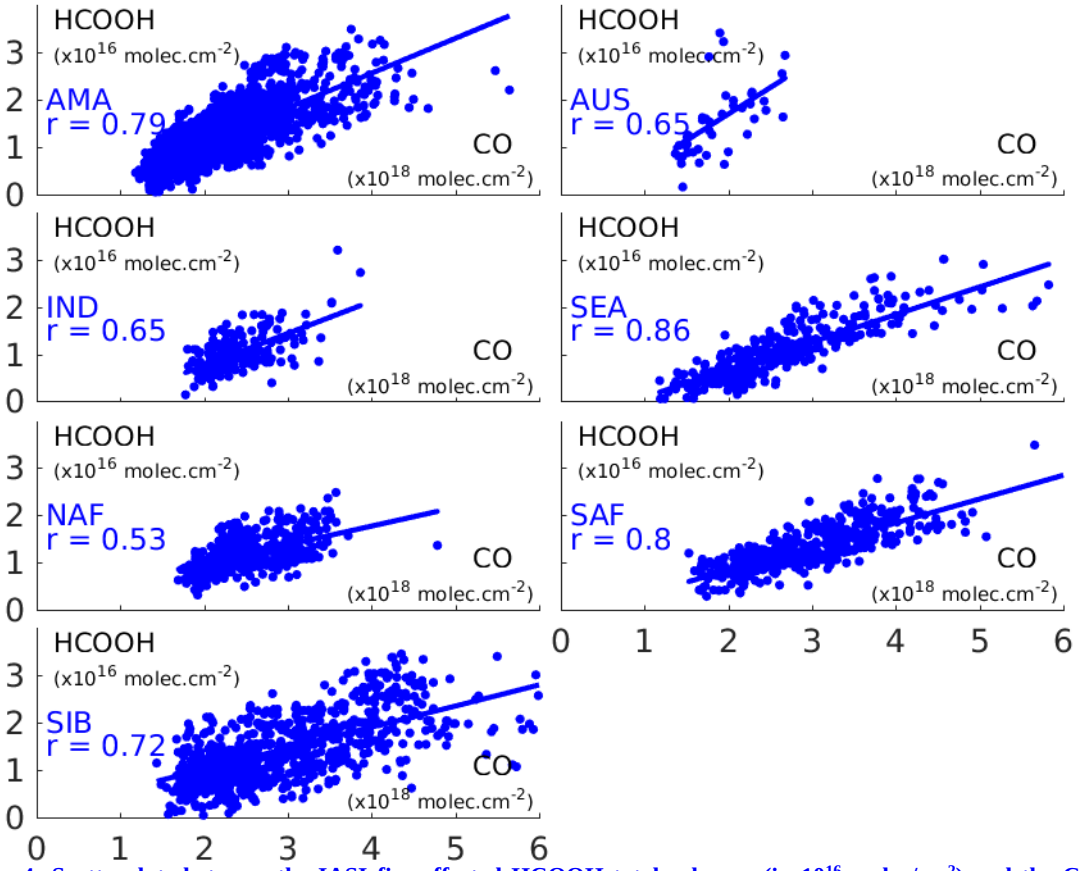

Figure 4: Scatterplots between the IASI fire-affected HCOOH total columns (in 10^{16} molec/cm^2) and the CO total columns (in 10^{18} molec/cm^2) over the seven regions (AMA=Amazonia, AUS=Australia, IND = India, SEA = Southern East Asia, NAF= Northern Africa, SAF= Southern Africa, SIB= Siberia).The linear regression is represented by the blue line and the correlation coefficient is also provided for each region.

Reviewer 2

General Comments
This manuscript presents IASI measurements of formic acid between 2008 and 2014, and uses these data to determine enhancement ratios from biomass burning emissions over seven regions. HCOOH and CO total columns, MODIS fire counts, and ECMWF surface wind speeds are combined to identify enhancements due to biomass burning. Correlations between HCOOH and CO total columns are used to calculate the enhancement ratio in each region. These results suggest that production of HCOOH by Siberian forest fires may be underestimated by 60%, and provide some insights into sources and sinks of HCOOH in other regions studied.
The manuscript provides a useful contribution to the field, but is somewhat qualitative and speculative in places, as noted by the other reviewer. It also has many distracting grammatical errors and should be carefully reviewed and revised to correct these and to improve the clarity of the writing. I recommend publication in ACP after the comments below are addressed.

The authors would like to thank reviewer 2 for his careful reading of the manuscript and for his thorough review. A detailed point by point reply (in blue) is provided hereafter.
As suggested by the first reviewer, an additional work has been done by using backward trajectories from HYSPLIT and land cover information from MODIS.
Moreover the text has been revised. Thus, in addition to our answers, we suggest that the reviewer reads the revised manuscript since Sect. 5.1 and 5.2 were largely rewritten.

A lot of MODIS hotspots have been studied in this paper, in total it represents 9628 hotspots. It is difficult to calculate backward trajectories for each hotspot, especially as different altitude ranges need to be tested since the vertical sensitivity of IASI (CO & HCOOH) is located in the free troposphere.
However, illustrative tests were done to show the distinct origins of the air masses at different locations, periods of the year and altitudes of the plume. Specifically, 5 hotspots have been chosen randomly for each region and 3 different altitudes have been selected: 500 m (thus close to the surface), 2000 m and 5000 m (representing the free troposphere). In total, this represents 105 trajectories.
These trajectories show that the air masses initialized at 500 and 2000m are mainly influencing by air masses close to the surface, confirming an origin near the source of our IASI fire-affected columns. It also shows the difficulty to estimate the origin of the air masses without an accurate knowledge of the altitude of the plumes.
These trajectories were plotted through the HYSPLIT online service:

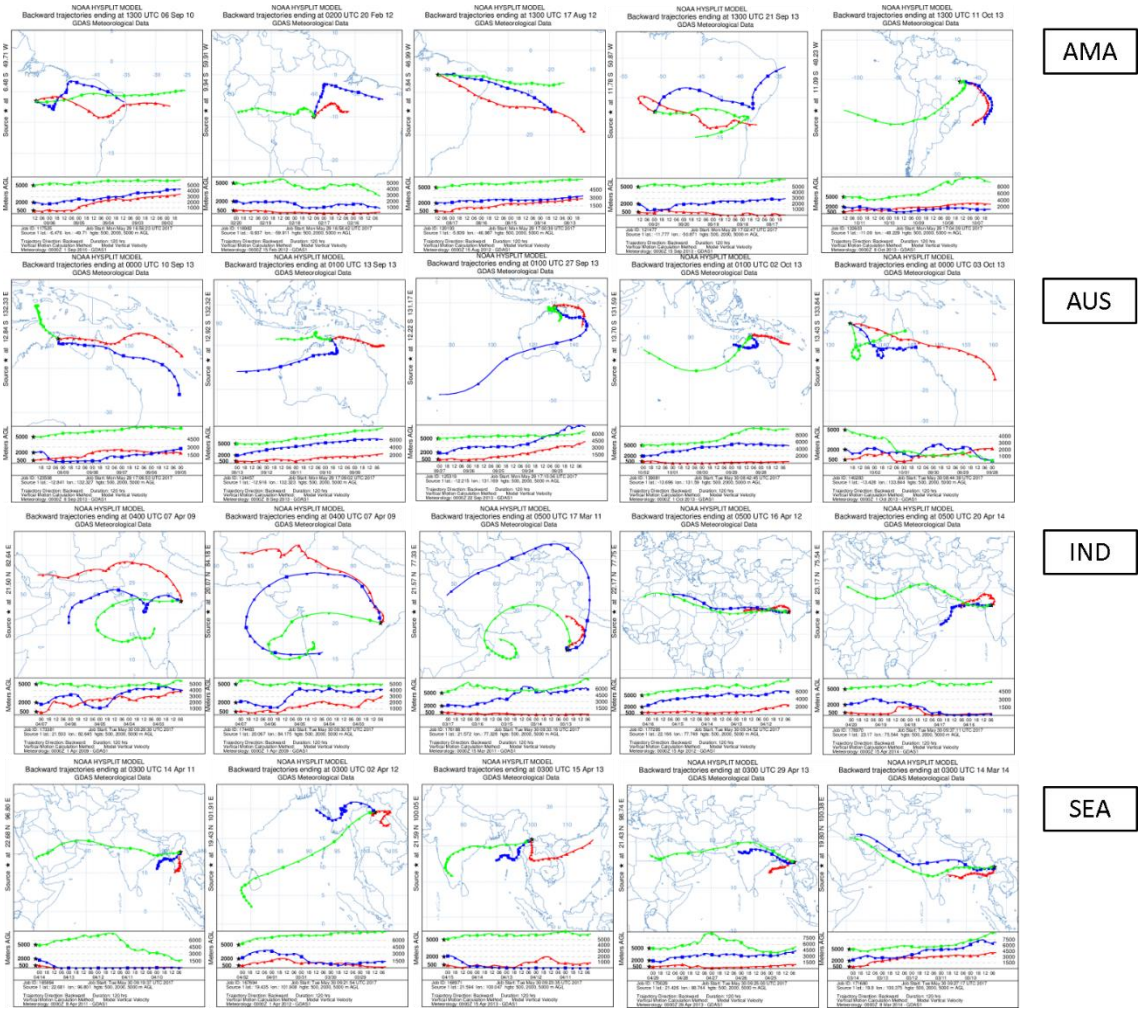

Fig 1. 5-day backward trajectories from HYPSLIT online service calculated at 3 altitudes: 500 m (red), 2000 m (blue) and 5000 m (green), for 5 hotspots chosen randomly over the 7 regions studied in the paper. The parameters characterizing each MODIS hotpots are summarized in the following table. The meteorological fields are from GDAS at 1°×1° horizontal resolution.

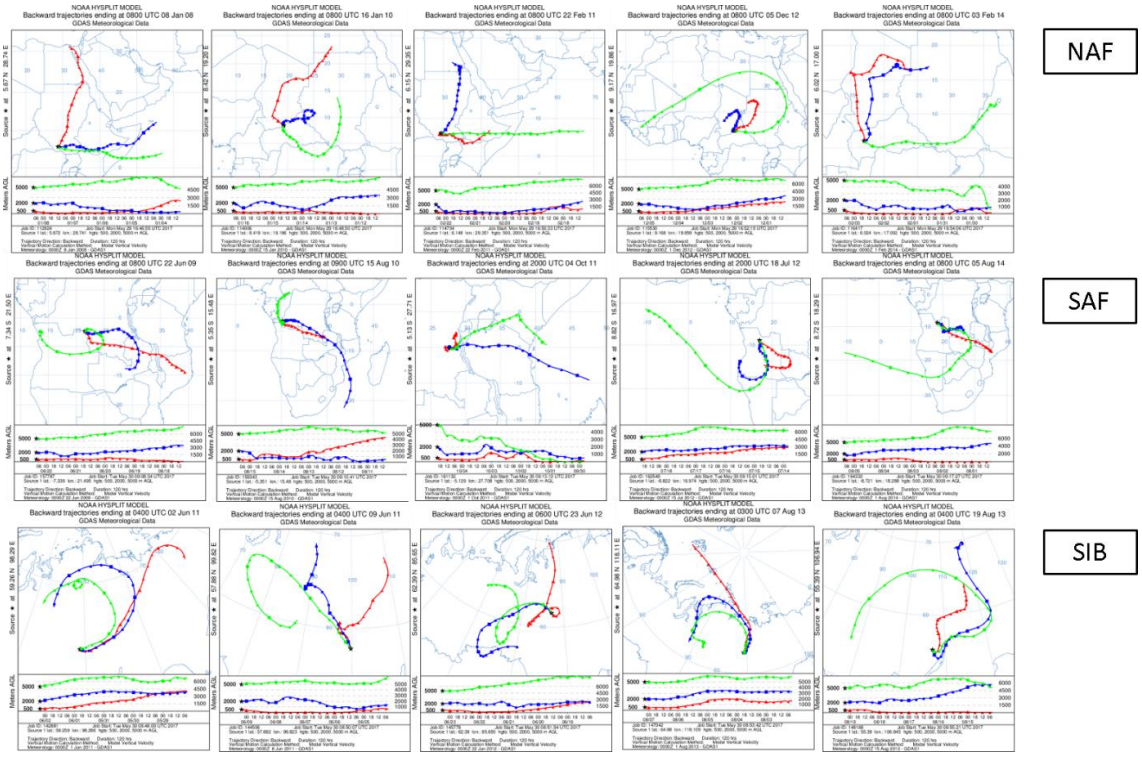

Fig 1. Continue

Tab. Characteristic of each MODIS hotspot used for the trajectories plotted in the previous figure. The dates, the time recorded by the instrument and the coordinates for each hotspot are written.

AMA
20100906 / hour (UTC)=13 / lat=-6.476 - lon=-49.71
20120220 / hour (UTC)=2 / lat=-9.937 - lon=-59.911
20120817 / hour (UTC)=13 / lat=-5.839 - lon=-46.987
20130921 / hour (UTC)=13 / lat=-11.777 - lon=-50.871
20131011 / hour (UTC)=13 / lat=-11.09 - lon=-48.229
AUS
20130910 / hour (UTC)=0 / lat=-12.841 - lon=132.327
20130913 / hour (UTC)=1 / lat=-12.916 - lon=132.323
20130927 / hour (UTC)=1 / lat=-12.215 - lon=131.169
20131002 / hour (UTC)=1 / lat=-13.696 - lon=131.59
20131003 / hour (UTC)=0 / lat=-13.428 - lon=133.844
IND
20090407 / hour (UTC)=4 / lat=21.503 - lon=82.645
20090407 / hour (UTC)=4 / lat=20.067 - lon=84.175
20110317 / hour (UTC)=5 / lat=21.572 - lon=77.328
20120416 / hour (UTC)=5 / lat=22.166 - lon=77.749
20140420 / hour (UTC)=5 / lat=23.17 - lon=75.544
SEA
20110414 / hour (UTC)=3 / lat=22.681 - lon=96.801
20120402 / hour (UTC)=3 / lat=19.435 - lon=101.908
20130315 / hour (UTC)=3 / lat=21.594 - lon=100.047
20130329 / hour (UTC)=3 / lat=21.426 - lon=98.744
20140314 / hour (UTC)=3 / lat=19.8 - lon=100.375

NAF
20080108 / hour (UTC)=8 / lat=5.672 - lon=28.741
20100116 / hour (UTC)=8 / lat=8.419 - lon=19.196
20110222 / hour (UTC)=8 / lat=6.148 - lon=29.351
20121205 / hour (UTC)=8 / lat=9.168 - lon=19.859
20140203 / hour (UTC)=8 / lat=6.024 - lon=17.002
SAF
20090622 / hour (UTC)=8 / lat=-7.339 - lon=21.495
20100815 / hour (UTC)=9 / lat=-5.351 - lon=15.48
20111004 / hour (UTC)=20 / lat=-5.129 - lon=27.708
20120718 / hour (UTC)=20 / lat=-8.822 - lon=16.974
20140805 / hour (UTC)=8 / lat=-8.721 - lon=18.288
SIB
20110602 / hour (UTC)=4 / lat=59.259 - lon=98.286
20110609 / hour (UTC)=4 / lat=57.882 - lon=99.823
20120623 / hour (UTC)=6 / lat=62.39 - lon=85.655
20130807 / hour (UTC)=3 / lat=64.98 - lon=118.109
20130819 / hour (UTC)=4 / lat=55.39 - lon=106.945

We have added the sentences (in bold) in our Section 5.1.2:
"A few backward trajectories (along 5 days, not shown) have been calculated for our hotspots with the online version of the HYSPLIT atmospheric transport and dispersion modeling system (Rolph, 2017). These trajectories, initialized at different altitudes, confirm a main origin close to the surface of our IASI fire-affected columns. It is however impossible to properly compare the origin of the air masses with previous studies as our studied period (2008-2014) or our studied fires do not necessarily match with plumes described in other publications. It is also difficult to estimate the age of our studied air masses by gathering the plumes during a 7-yr period and without an accurate knowledge of the altitude of the plumes."

And:

"One possible explanation is the multi-origin of the plumes studied by Rinsland et al. (2006), since, based on their backward trajectories, their plumes could be influenced by biomass burning originating from Southern Africa and/or from Southern America. **The travel during the few days across the Atlantic Ocean may explain the change in their ER$_{(HCOOH/CO)}$."**

With the corresponding reference:
Rolph, G.D.: Real-time Environmental Applications and Display sYstem (READY) Website (http://www.ready.noaa.gov). NOAA Air Resources Laboratory, College Park, MD, 2017.

We also have discovered that the information about the type of vegetation was available in the MODIS products.
In "Section 3. MODIS" we have added this paragraph:
"To characterize each MODIS hotspot by the type of fuel burned, the Global Mosaics of the standard MODIS land cover type data product (MCD12Q1) in the IGBP Land Cover Type Classification (Friedl et al., 2010; Channan et al., 2014) with a 0.5° × 0.5° horizontal resolution has also been used (http://glcf.umd.edu/data/lc/). As the annual variability in this product is limited (not shown) and since the period available (from 2001 to 2012) does not fully match

the period of the IASI mission, only the data for 2012 have been used. Whitburn et al. (2017) have also used this MCD12Q1 product to determine their IASI-derived NH_3 enhancement ratios by vegetation types."

With the corresponding references:
Channan, S., Collins, K., and Emanuel, W. R.,Global mosaics of the standard MODIS land cover type data. University of Maryland and the Pacific Northwest National Laboratory, College Park, Maryland, USA, 2014.
And
Friedl, M. A., Sulla-Menashe, D., Tan, B., Schneider, A., Ramankutty, N., Sibley, A. and Huang, X., MODIS Collection 5 global land cover: Algorithm refinements and characterization of new datasets, 2001-2012, Collection 5.1 IGBP Land Cover, Remote Sensing of Environment, 114 , 168–182, doi:10.1016/j.rse.2009.08.016, 2010.
And
Whitburn, S., Van Damme, M., Clarisse, L., Hurtmans, D., Clerbaux, C., and Coheur, P.-F.: IASI-derived NH3 enhancement ratios relative to CO for the tropical biomass burning regions, Atmos. Chem. Phys. Discuss., https://doi.org/10.5194/acp-2017-331, in review, 2017.

We have also added this sentence in Section 4.2:
"The classification of the vegetation from the MODIS product has also been used for a detailed analysis of the enhancement ratios for these regions (Fig. 1)."
And Fig. 1 has been modified as below:

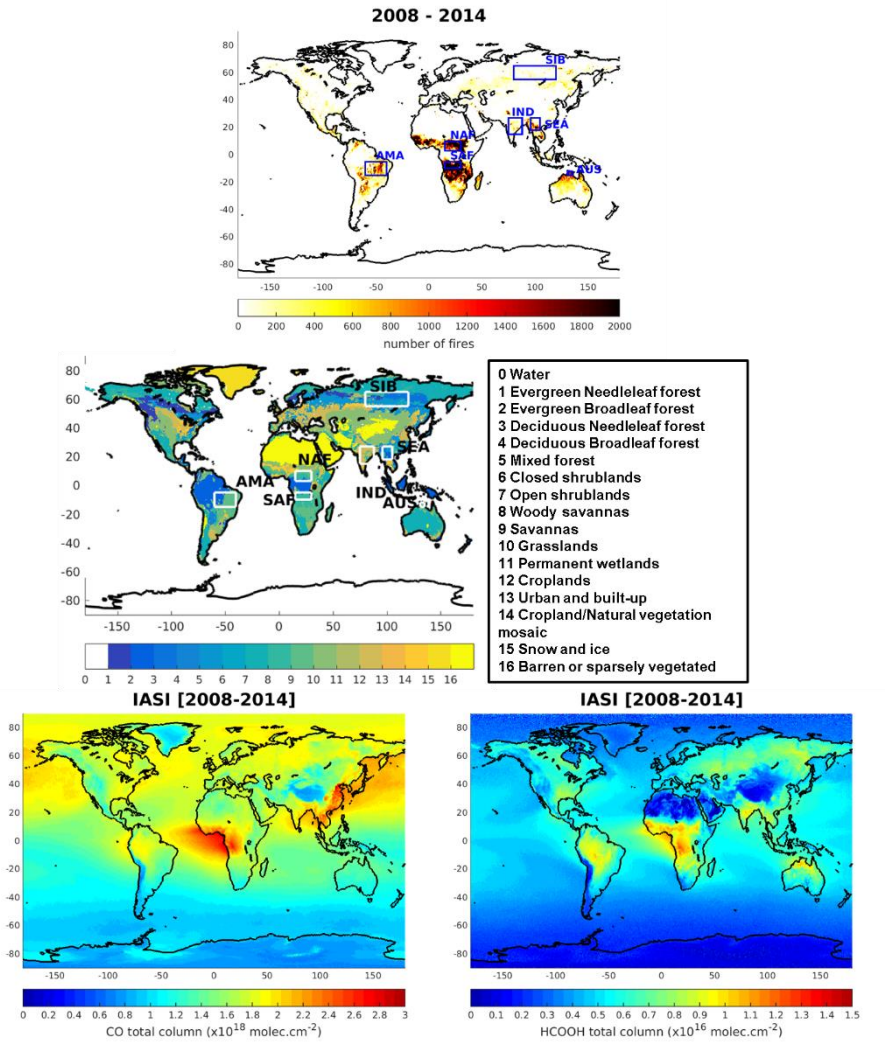

Figure 1: Top: Number of MODIS fire hotspots with a confidence percentage higher or equal to 80%, averaged on a 0.5°×0.5° grid, for the period between 2008 and 2014. The blue boxes are the regions studied in this work. Middle: Classification of the land cover type from MODIS on the same grid and highlighting the studied regions in white. Each number corresponds to the type of vegetation. Only the data between 64°S and 84°N are available. Bottom: The IASI CO total column distribution (left) and the IASI HCOOH total column distribution (right), averaged between 2008 and 2014 and on the same grid.

Section 5.2 was also rewritten and now named "5.2. Analysis based on the type of vegetation" since ER (HCOOH/CO) by biome have also been added in Table 3 as below:

Table 3. Enhancement ratio of HCOOH relative to CO (mol/mol) with its standard deviation and enhancement ratio of HCOOH relative to CO (mol/mol) by biome with its standard deviation calculated in this work. For each enhancement ratio by biome, the correlation coefficient and the number of MODIS hotspots are provided. The enhancement ratios are compared to emission ratios calculated from emission factors given in the literature for the seven studied regions. For the calculation of these emission ratios, the emission factors of CO for the corresponding fuel type given in Akagi et al. (2011) are used. Emission ratios of HCOOH relative to CO (mol/mol) calculated from the emission factors of HCOOH given in Akagi et al. (2011) for the corresponding fuel type are also provided.

Region	**Enhancement Ratio to CO (mol/mol) – this work**	**Enhancement Ratio to CO (mol/mol)[1] by biome[2] – this work**	Emission Ratio to CO (mol/mol) calculated from EF_{HCOOH} given in literature and using EF_{CO} from Akagi et al. (2011)	Instrument used
AMA	**$7.3\times10^{-3} \pm 0.08\times10^{-3}$**	**$6.3\times10^{-3} \pm 0.22\times10^{-3}$ (Evergreen Broadleaf forest, r=0.81, n = 454)** **$3.0\times10^{-3} \pm 0.81\times10^{-3}$ (Open shrubland, r=0.91, n = 5)** **$7.0\times10^{-3} \pm 2.47\times10^{-3}$ (Woody savanna, r=0.63, n = 14)** **$7.6\times10^{-3} \pm 0.09\times10^{-3}$ (Savanna, r=0.79, n = 3909)** **$8.4\times10^{-3} \pm 0.39\times10^{-3}$ (Grassland, r=0.88, n = 143)** **$4.6\times10^{-3} \pm 0.35\times10^{-3}$ (Cropland, r=0.88, n = 54)**	1.8×10^{-3} – Tropical forest (Yokelson et al., 2007 ; 2008)[3] 2.7×10^{-3} – Savanna (Yokelson et al., 2007 ; 2008)[3] 2.0×10^{-3} – Savanna (Akagi et al., 2011) 5.2×10^{-3} – Tropical forest (Akagi et al., 2011)	Airborne FTIR (Yokelson et al., 2007) ; laboratory (Yokelson et al., 2008) catalogue
AUS	**$11.1\times10^{-3} \pm 1.37\times10^{-3}$**	**$5.7\times10^{-3} \pm 2.55\times10^{-3}$ (Woody savanna, r=0.6, n = 11)** **$11.2\times10^{-3} \pm 1.49\times10^{-3}$ (Savanna, r=0.65, n = 80)**	2.0×10^{-3} – Savanna (Akagi et al., 2011)	catalogue
IND	**$6.8\times10^{-3} \pm 0.44\times10^{-3}$**	**$6.6\times10^{-3} \pm 0.77\times10^{-3}$ (Woody savanna, r=0.65, n = 103)** **$6.2\times10^{-3} \pm 0.62\times10^{-3}$ (Cropland, r=0.58, n = 198)** **$8.8\times10^{-3} \pm 1.19\times10^{-3}$ (Cropland/Natural vegetation mosaic, r=0.85, n =23)**	2.0×10^{-3} – Savanna (Akagi et al., 2011) 2.7×10^{-3} – Extratropical forest (Akagi et al., 2011) 6.0×10^{-3} – Cropland (Akagi et al., 2011)	catalogue
SEA	**$5.8\times10^{-3} \pm 0.15\times10^{-3}$**	**$5.6\times10^{-3} \pm 0.20\times10^{-3}$ (Evergreen Broadleaf forest, r=0.83, n = 334)**	2.0×10^{-3} – Savanna (Akagi et al., 2011) 2.7×10^{-3} – Extratropical forest (Akagi et al., 2011) 6.0×10^{-3} – Cropland (Akagi et al., 2011)	catalogue

		$6.3\times10^{-3} \pm 0.66\times10^{-3}$ (Mixed forest, r=0.76, n = 70) **$6.2\times10^{-3} \pm 0.38\times10^{-3}$ (Woody savanna, r=0.86, n = 99)** **$7.1\times10^{-3} \pm 0.99\times10^{-3}$ (Cropland/Natural vegetation mosaic, r=0.84, n =23)**		
NAF	**$4.0\times10^{-3} \pm 0.19\times10^{-3}$**	**$3.4\times10^{-3} \pm 0.63\times10^{-3}$ (Evergreen Broadleaf forest, r=0.52, n = 78)** **$3.3\times10^{-3} \pm 0.28\times10^{-3}$ (Woody savanna, r=0.44, n = 569)** **$4.4\times10^{-3} \pm 0.29\times10^{-3}$ (Savanna, r=0.59, n = 441)** **$22.6\times10^{-3} \pm 11.06\times10^{-3}$ (Cropland/Natural vegetation mosaic, r=0.67, n = 7)**	2.0×10^{-3} – Savanna (Akagi et al., 2011)	catalogue
SAF	**$5.0\times10^{-3} \pm 0.13\times10^{-3}$**	**all hotspots are woody savanna**	3.3×10^{-3} – Tropical forest (Sinha et al., 2004)[4] 4.8×10^{-3} – Savanna (Sinha et al., 2004)[4] 4.1×10^{-3} – Tropical forest (Yokelson et al., 2003) 6.0×10^{-3} – Savanna (Yokelson et al., 2003) 13×10^{-3} – Tropical forest (Rinsland et al., 2006) 19.2×10^{-3} – Savanna (Rinsland et al., 2006) 2.0×10^{-3} – Savanna (Akagi et al., 2011) 5.2×10^{-3} – Tropical forest (Akagi et al., 2011)	Airborne FTIR Airborne FTIR ACE-FTS catalogue
SIB	**$4.4\times10^{-3} \pm 0.09\times10^{-3}$**	**$4.0\times10^{-3} \pm 0.31\times10^{-3}$ (Evergreen Needleaf forest, r=0.63, n = 245)** **$3.6\times10^{-3} \pm 0.16\times10^{-3}$ (Deciduous Needleaf forest, r=0.66, n = 659)** **$3.4\times10^{-3} \pm 0.18\times10^{-3}$ (Mixed forest, r=0.57, n = 759)**	2.7×10^{-3} – Boreal forest (Akagi et al., 2011)	catalogue

	$6.6\times10^{-3} \pm 0.48\times10^{-3}$ (Open shrubland, r=0.76, n = 143) **$6.0\times10^{-3} \pm 0.41\times10^{-3}$ (Woody savanna, r=0.76, n = 155)** **$3.8\times10^{-3} \pm 0.65\times10^{-3}$ (Permanent wetland, r=0.6, n = 63)**

[1] Only the enhancement ratio to CO calculated from a scatterplot with a correlation coefficient higher than 0.4 are reported.
[2] The type of vegetation is defined by the land cover type data product (MCD12Q1).
[3] The EF_{HCOOH} were corrected based on the comment from Yokelson et al. (2013) (EF_{HCOOH} used: 0.281 for Yokelson et al. (2007); 0.2767 for Yokelson et al. (2008)).
[4] The mean of both EF_{HCOOH} values provided in Sinha et al. (2004) were used for our $EmR_{HCOOH/CO}$ calculation

We have added these sentences at the end of the Section 5.2:
"In addition to the $EmR_{(HCOOH/CO)}$ calculated from the EF_{HCOOH} given in the literature, a classification for our $ER_{(HCOOH/CO)}$ has also been done, based on the data from the MCD12Q1 product. As each hotspot is associated with a land cover value defined by the MCD12Q1 product, enhancement ratios by biome have been calculated. The limitations of this dataset are its coarse resolution (0.5° × 0.5°) and the lack of seasonal variation. It gives however a supplementary information on the type of fuel burned identified by MODIS. The corresponding $ER_{(HCOOH/CO)}$ are provided in Table 3. Only the values calculated from a scatterplot with a correlation coefficient higher than 0.4 are reported."

And

"In general, the $ER_{(HCOOH/CO)}$ calculated for a specific biome varies with the regions. This shows that the type of vegetation is not the only factor influencing the $ER_{(HCOOH/CO)}$. The ongoing chemistry within a plume is important and the age of the air masses impact the level of HCOOH and CO in the plumes."

We have also added these sentences in the abstract:
"An additional classification of the enhancement ratios by type of fuel burned is also provided, showing a diverse origin of the plumes sampled by IASI, especially over Amazonia and Siberia. The variability in the enhancement ratios by biome over the different regions show that the levels of HCOOH and CO do not only depend on the fuel types."
And in the conclusion:
"Finally, the estimation of the $ER_{(HCOOH/CO)}$ calculated by the type of vegetation burned, as referenced in the MODIS product, varies with the regions. This shows that other parameters than the type of fuel burned also influence the $ER_{(HCOOH/CO)}$."

Specific Comments
Page 1, line 1 – The title is awkwardly phrased. Why just a "Possibility" for IASI to detect HCOOH in biomass burning plumes? "document" should be replaced by "measure" or "detect". A better title might be something like: "Detection of HCOOH from biomass burning plumes by the Infrared Atmospheric Sounding Interferometer"
The title is now:
"Determination of enhancement ratios of HCOOH relative to CO in biomass burning plumes by the Infrared Atmospheric Sounding Interferometer (IASI)."

Page 1, lines 25-27 – Make clear whether this underestimation for Siberian forest fires is in the IASI HCOOH or other studies or both. This seems rather speculative based on the results presented in the paper.
This information has been deleted from the abstract but we have added these sentences (in bold) in the conclusions:
"The underestimation by 60% over Siberia is consistent with conclusions given in R'Honi et al. (2013). **The calculation of the $ER_{(HCOOH/CO)}$ by biome shows that Siberian plumes are related to the burning of six different vegetation classes. The underestimation reported is thus difficult to confirm without the use of a chemical transport model."**

We have also written in Section 5.2:
"These hypotheses in biased emissions and/or secondary production need, however, to be verified with modeling studies."

Page 1, lines 27-29 – Rewrite this last sentence for clarity.
Done. Now it reads:
"In comparison **with referenced emission ratios**, it is also shown that the selected agricultural burning plumes captured by IASI over India and Southern East Asia correspond to recent plumes where the chemistry or the sink does not occur."

Page 5, line 185 – Why is 1.44 m/s used as a threshold?
As explained in the following sentence: "This value of 1.44 m/s for the surface wind speed corresponds to the 25th percentile of the distribution of the three regions characterized by the lowest surface wind speed (Fig. 3)."

Page 6, lines 210-212 – Please clarify this discussion. It is not clear how a better detection limit "minimizes the bias with the lowest columns", nor what suggests "a negligible effect of the low column biases".
We agreed it was confusing. Now the sentences are (the modifications are highlighted in bold):

"Nevertheless, in order to investigate the possible impact of the overestimation in the lower columns **and the underestimation in the higher columns** on the calculated ratios, a test was performed, by using only HCOOH columns with a thermal contrast larger than 10K. Indeed, the increase in the thermal contrast (i.e. the temperature difference between the surface and the first layer in the retrieved profile) leads to **reducing** the detection limit as shown in Pommier al. (2016**). This enhancement of the detection level helps to minimize the bias in the retrieved total columns as explained in Crevoisier et al. (2014). For the analysis performed here, similar slopes and correlation coefficients were generally calculated**, suggesting a negligible effect of this parameter on the biases. The only exception is an increase in $ER_{(HCOOH/CO)}$ over Siberia ($6.5\times10^{-3} \pm 0.19\times10^{-3}$ mol/mol when using only IASI measurements with TC above 10K against 4.4×10^{-3} mol/mol $\pm 0.09\times10^{-3}$ in Table 2). **It is worth noting that only 48% of the selected scenes remain over Siberia when applying this filter on thermal contrast (60% for SEA, 77% for AMA, 80% for SAF, 83% for AUS and NAF, and 89% for IND). This implies that the statistics on the fire emissions in the higher latitudes of Siberia is dominated by measurements with a low thermal contrast and thus with HCOOH total columns with higher uncertainties. However, the limited changes in slopes and correlation coefficients give** us confidence that the results presented in Table 2 are **representative**."

We also have added this reference:
Crevoisier, C., Clerbaux, C., Guidard, V., Phulpin, T., Armante, R., Barret, B., Camy-Peyret, C., Chaboureau, J.-P., Coheur, P.-F., Crépeau, L., Dufour, G., Labonnote, L., Lavanant, L., Hadji-Lazaro, J., Herbin, H., Jacquinet-Husson, N., Payan, S., Péquignot, E., Pierangelo, C., Sellitto, P., and Stubenrauch, C.: Towards IASI-New Generation (IASI-NG): impact of improved spectral resolution and radiometric noise on the retrieval of thermodynamic, chemistry and climate variables, Atmos. Meas. Tech., 7, 4367-4385, doi:10.5194/amt-7-4367-2014, 2014.

Page 6, para 3 – This is a long paragraph, written in a way that is hard to follow. Please revise for clarity. e.g., lines 224-228 – Explanations are also not clear here. Please explain why the results suggest that the plume "encountered a limited secondary production or a low sink as deposition or reaction with OH" and why the faster decay of HCOOH relative to CO, suggests rapid advection of the plumes.
The section has been rewritten. Please refer to the revised manuscript.

About lines 224-228, now it reads (the changes are in bold):
"Since these $ER_{(HCOOH/CO)}$ from previous studies and the $EmR_{(HCOOH/CO)}$ from Sinha et al. (2003) agree with our $ER_{(HCOOH/CO)}$, and since HCOOH has a short lifetime, this may suggest that the selected plumes measured by IASI from 2008 to 2014 and those sampled by Vigouroux et al. (2012) and Coheur et al. (2007), encountered a limited secondary production or a low sink as deposition or reaction with OH in the troposphere during their transport**. To quantify the role of the chemistry or of the deposition within the plumes, a modeling work should be performed. This is however beyond the scope of this paper.**
Another important point is that the decay of HCOOH is faster than for CO**. As our $ER_{(HCOOH/CO)}$ is similar to the $ER_{(HCOOH/CO)}$ from the other studies and to the $EmR_{(HCOOH/CO)}$ given in Sinha et al. (2003), this could suggest that all these plumes (from our study, from Vigouroux et al. (2012) and Coheur et al. (2007))** are rapidly advected in the troposphere".

And line 237 – How would the impact of the difference in the geometry of sampling be accounted for in a proper comparison between ACE-FTS and IASI?
The sentences were confusing. The sentences have been changed as below:
"It is worth noting that the ACE-FTS instrument used in their study works in a limb solar occultation mode. This means that the atmospheric density sampled by the instrument is larger than the one measured by the nadir geometry with IASI. However, the difference in geometry cannot explain why we find an agreement with the ACE-FTS measurements values reported by Coheur et al. (2007) and a disagreement with those from Rinsland et al. (2006). Part of the difference could be associated with the difference in the assumptions used in both retrievals (e.g. the a priori)."

Line 239 – Where were the plumes sampled by Yokelson et al.?
The plumes were over Zambia, Zimbabwe and South Africa. This information is now included in the sentence (in bold):
"The $ER_{(HCOOH/CO)}$ from our work is also 15% lower than the $EmR_{(HCOOH/CO)}$ in Yokelson et al. (2003) ($5.9\times10^{-3} \pm 2.2\times10^{-3}$ mol/mol) **who calculated their value within plumes over Zambia, Zimbabwe and South Africa**."

Page 7, lines 243-244 – What was the approach developed by Chaliyakunnel et al. (2016) to determine pyrogenic ER(HCOOH/CO)? It is not clear what is meant "by reducing the impact of the mix with the ambient air".

An explanation of their approach is now added (in bold):

"**To do so, they calculated the $ER_{(HCOOH/CO)}$ in the vicinity of fire count from MODIS (averaged in a cell having the resolution of the GEOS-Chem model, i.e. 2°× 2.5°) and they differentiated this value with a background $ER_{(HCOOH/CO)}$ defined by the concentrations distant from these fires.** They concluded that their most reliable value on the amount of HCOOH produced from fire emissions was obtained for African fires."

Page 7, lines 269-271 – Revise this poorly written paragraph. It is not clear what is meant by either sentence.

As explained as introduction of our answers, section 5.2 was rewritten and the title of section has been changed.

To answer the question about lines 269-271, the new lines are (the changes are in bold):

"5.2. Analysis based on the type of vegetation

We have complemented our comparison of the enhancement ratios **by comparing our ratios to emissions ratios calculated** from emission factors found in literature. The main argument to perform such comparison is the lack of measurements of enhancement ratios over IND and SEA. **Furthermore, such comparison from emission factors facilitates an analysis based on hypothesis about the type of vegetation burned."**

Page 7, lines 275-279 – Why can't the decay be taken into account by considering the exponential decrease between emission and detection using relative lifetimes, e.g., Viatte et al. (2015) and references therein?

Each MODIS hotspot is characterized by a mean CO total column and a mean HCOOH total column. These averages are calculated along 5 hours. During 5 hours, the chemistry may already occur and it is the reason why we have written that the decay of these compounds could not be taken into account in our methodology.

Moreover, without to know the accurate altitude of the plumes, it is challenging to calculate the age of the air masses.

Sections 5.1 and 5.2 – Both sections discuss enhancement ratios and emission ratios, including comparisons with other studies, e.g., on page 8, there is additional discussion of ER although the title suggests that Section 5.2 is about EmR. These sections could be more clearly differentiated.

Both sections have been changed.

Now there are:

5. Analysis of the data over the fire regions

5.1. Determination of the enhancement ratios

5.1.1 General analysis

5.1.2 Analysis over each region

5.2. Analysis based on the type of vegetation

Page 9, lines 358-359 – Arguably, such an intercomparison could have been included in this study.

An inter-comparison has to be done but it is beyond the scope of this paper. It will be a subject for a next study. It is the reason why it was mentioned in the conclusion.

Technical Corrections
Page 1, line 19 – add comma after "(MODIS)"
Done

Page 1, line 26 – add comma after "forest fires"
The sentence has been deleted.

Page 1, line 34 – delete "for"
Done

Page 2, line 46 – Rewrite this sentence. Not clear what is meant by "as on the oxidizing power..."
A complementary information is now provided. The changes are shown in bold:
"… on the oxidizing **capacity** of the atmosphere **(i.e. the chemistry of OH in cloud water - Jacob, 1986; the heterogeneous oxidation of organic aerosols - Paulot et al., 2011**)"

and we have added this reference:
Jacob, D.: Chemistry of OH in remote clouds and its role in the production of formic acid and peroxymonosulfate, J. Geophys. Res., 91, 9807–9826, 1986.

Page 2, line 55 – "hence depend on"
Corrected

Page 2, line 67 – change "as with" to "including" or "such as"
"Including" is now used.

Page 2, line 69 – delete "with the"
Done

Page 2, line 70 – "Atmospheric Chemistry Experiment – Fourier Transform Spectrometer (ACE-FTS)"
Changed

Page 2, line 72 – I think this means "(MIPAS) limb instrument, which is sensitive to altitudes down to ~ 10 km" (rather than only sensitive at 10 km)
Grutter et al. (2010) – the cited reference – shows distributions and time-series at 10 km. Most of their profiles start at 8 km, and thus we kept the sentence:
"… Michelson Interferometer for Passive Atmospheric Sounding (MIPAS) limb instrument which is sensitive to around 10 km (Grutter et al., 2010)."

Page 2, line 74 – "compared to ground-based and airborne"
Corrected.

Page 2, line 75 – "allows observation of remote regions"
"which allows observing remote regions" is now changed by "allows observation of remote regions".

Page 2, line 77 – "ratios of HCOOH relative to CO over"
Changed.

This change has also done in the title of the tables.

Page 3, lines 93-94 – add space before K, as done for other units like km, cm-1, etc.
Done

Page 3, line 97 – Isn't the lifetime of CO closer to two months than several weeks?
The lifetime depends on the season and on the location. We clarified this point by changing "several weeks" by "a few weeks to a few months depending on latitude and time of year."

Page 3, line 113 – "in more detail"
Corrected

Page 3, lines 117-118 – "which is less than 35% for total columns smaller than..."
Changed

Page 4, line 123 – "hotspots"
"s" has been added.

Page 4, line 123 – MODIS has already been defined
That is correct. Thank you for noticing it.

Page 4, line 129 – "which, for each detected fire pixel, includes the ..."
Changed.

Page 4, line 132 – Last sentence doesn't need to be a separate paragraph.
Changed.

Page 4, line 141 – "most active in terms of actual fires but are still of interest. The first ..." These four sentences about importance of biomass burning in India and Siberia could also be rewritten for clarity.
The sentence has been changed as:
"Among these regions, India and Siberia do not represent the most active regions in terms of number of fires. It seemed however important to also investigate them."

Page 4, line 144 – "over some years, such as during summer 2010"
Changed

Page 4, line 154 – "(correlation coefficient, r, from"
Changed

Page 4, line 155 – "the impact of sources other than biomass burning"
Changed.

Page 4, line 156 – "also have"
Changed

Page 4, line 160 – "The large region selected over Siberia"
Changed

Page 4, line 161 – "other regions, such as polluted"

Changed

Page 5, line 170 – add comma after “criteria”
Done

Page 5, line 171 – “in Table 1. The smaller correlation coefficients, i.e., less than 0.7, are found”
Changed

Page 5, line 172 – “the HCOOH and CO columns”
Changed

Page 5, line 178 – “assign” rather than “attribute” ?
Changed

Page 5, line 179 – ECMWF has already been defined
It was not defined previously, except in the abstract. Thus we have decided to keep the definition in this line.

Page 5, line 182 – “(r close to 0.8)”
“r” has been added.

Page 5, line 183 – Clarify that the low mean and median refer to surface wind speed. Also rewrite the sentence on line 184 for clarity.
The sentence has been changed as:
“IND has also a low mean and median **surface wind speed** but the distribution of **this** surface wind speed **over IND** is more spread out than for **AMA, SEA and SAF**.”

Page 5, line 186 and elsewhere through the manscript– “in Table 2” ? Does ACP accept Tab. as an abbreviation for Table?
“Tab” has been changed by “Table” everywhere through the manuscript.

Page 5, line 197 – “than using only the columns”
Changed

Page 5, line 198 – “for each measurement pair”
Corrected

Page 6, line 201 – “so comparison with previous work is ... over another”
Corrected.

Page 6, line 203 – should globally be generally?
“globally” was changed by “generally”.

Page 6, line 206 – “The effects of both biases are, however, limited”
The sentence has been changed as requested.

Page 6, line 211 – “an improved [or a lower?] detection limit”
That’s correct; in this case, improved means lower. To clarify it, we have changed “improve” by “reduce”. Now it reads:

"Indeed, the increase in the thermal contrast (i.e. the temperature difference between the surface and the first layer in the retrieved profile) leads to **reducing** the detection limit as shown in Pommier al. (2016)."

Page 6, line 222 – "same plume as"
Corrected

Page 6, line 231 – trajectories
Corrected

Page 6, line 235 – "reasons for the agreement"
The sentence has been changed:
"However, the difference in geometry cannot explain why we find an agreement with the ACE-FTS measurements values reported by Coheur et al. (2007) and a disagreement with those from Rinsland et al. (2006)."

Page 6, lines 241-242 – "Conversely, the … from IASI is twice that of Chaliyakunnel"
Changed. The sentence is now:
"**Conversely,** the $ER_{(HCOOH/CO)}$ retrieved **from IASI is twice that of** Chaliyakunnel et al. (2016) ($2.6\times10^{-3} \pm 0.3\times10^{-3}$ mol/mol)."

Page 7, line 247 – No need for a new paragraph here.
We have preferred to keep this new paragraph since it corresponds to the analysis of the results over NAF and the previous paragraphs are about SAF.

Page 7, line 248 – "worth noting"
"Reminding" is replaced by "noting" as requested.

Page 7, line 251 – "and that of Paton-Walsh (2005) may be explained"
Changed. The sentence is now: "The difference between our work a**nd that of Paton-Walsh (2005) may be explained** by the different origin of the probed plume."

Page 7, line 254 – quantify "quite uncertain"
The value is now given in text:
"… a quite uncertain value is reported **($4.5\times10^{-3} \pm 5.1\times10^{-3}$ mol/mol)**,…"

Page 7, line 280 – "For both the IND"
The comma has been deleted as requested.

Page 8, line 287 – Equation
Changed

Page 8, line 289 – "composed of tropical"
Page 8, line 292 – "composed of cropland"
Both were corrected.

Page 8, line 293 – "characterized by an"
Corrected.

Page 8, line 300 – "(2004) both used the same"

Changed.

Page 8, line 307 – "twice the value" [also specify whether ER or EmR from Akagi]
We agreed that this sentence was confusing. We changed "value" by "EmR". Now it reads:
"Over Northern Africa, our $ER_{(HCOOH/CO)}$ **is twice as large as** the **$EmR_{(HCOOH/CO)}$** provided by Akagi et al. (2011), probably due to the lower correlation found in our scatterplot."

Page 8, line 308 – "It is highly"
Changed.

Page 8, line 314 – "forest fire plumes"
Changed.

Page 9, line 336 – "difficulties ... are"
Corrected

Page 9, line 338 – "using satellite, airborne, or FTIR measurements"
Changed

Page 9, line 346 – "A very good agreement was found" in what? Specify.
The information has been added (in bold):
"A very good agreement **in $ER_{(HCOOH/CO)}$** was found over Amazonia, especially with the work done by Chaliyakunnel et al. (2016) who determinated pyrogenic $ER_{(HCOOH/CO)}$."

Page 9, line 349 – Replace "delicate" with a better description.
We replaced "delicate" by "complicated":
"The analysis over Australia is however **complicated** as our $ER_{(HCOOH/CO)}$ approximately corresponds…"

Page 9, line 355 – "a modelling study could be"
"work" has been replaced by "study".

Page 9, line 357 – times
"s" has been added.

Page 9, line 358 – "instruments such as"
"Such" has been added.

Page 10, line 367 – Isn't IASI an instrument, not a mission?
There are 3 similar instruments. So IASI is both an instrument and a long term mission.

Page 10, line 372 – "for free access"
Corrected

Page 10, lines 385 and 387 – Inconsistent formatting of references for the same journal.
Thanks for this observation. The doi was missing for the first reference. Now the references are:
Andrews, D. U., Heazlewood, B. R., Maccarone, A. T., Conroy, T., Payne, R. J., Jordan, M. J. T., and Kable, S. H.: Photo-tautomerization of acetaldehyde to vinyl alcohol: a potential route to tropospheric acids, Science, 337, 1203–1206, doi:10.1126/science.1220712, 2012.

Beirle, S., K. F. Boersma, U. Platt, M. G. Lawrence, and T. Wagner : Megacity emissions and lifetimes of nitrogen oxides probed from space, Science, 333, 1737–1739, doi:10.1126/science.1207824, 2011.

Page 17, caption line 2 – "over the 7 [seven] regions studied. IASI data are"
7 has been replaced by "seven".

Page 17 – Tab. or Table ?
As for your previous comment, "Tab" has been changed by "Table" everywhere through the manuscript.

Pages 18 and 19, table headings – "HCOOH/CO Enhancement/Emission Ratio ..." would be a better title
The table headings are:

Table 2. Enhancement ratio of HCOOH relative to CO (mol/mol) with its standard deviation compared to enhancement ratios of HCOOH relative to CO and emissions ratios of HCOOH reported in the literature for the seven studied regions.

Table 3. Enhancement ratio of HCOOH relative to CO (mol/mol) with its standard deviation and enhancement ratio of HCOOH relative to CO (mol/mol) by biome with its standard deviation calculated in this work. For each enhancement ratio by biome, the correlation coefficient and the number of MODIS hotspots are provided. The enhancement ratios are compared to emission ratios calculated from emission factors given in the literature for the seven studied regions. For the calculation of these emission ratios, the emission factors of CO for the corresponding fuel type given in Akagi et al. (2011) are used. Emission ratios of HCOOH relative to CO (mol/mol) calculated from the emission factors of HCOOH given in Akagi et al. (2011) for the corresponding fuel type are also provided.

Page 18, Table 3 – Left justify all the table entries
Done

Page 19, caption line 2 – "in the literature". Also, rewrite the full caption for conciseness and clarity, e.g., HCOOH/CO enhancement ratio, etc.
See our answer about the table headings.

Page 20, caption line 3 – "column distribution ... column distribution"
Corrected

Page 21, Figure 2 and page 22, Figure 4– Preferable to have units on the y-axis labels, rather than just in the caption.
Figs 2 and 4 now include units, as hereafter:

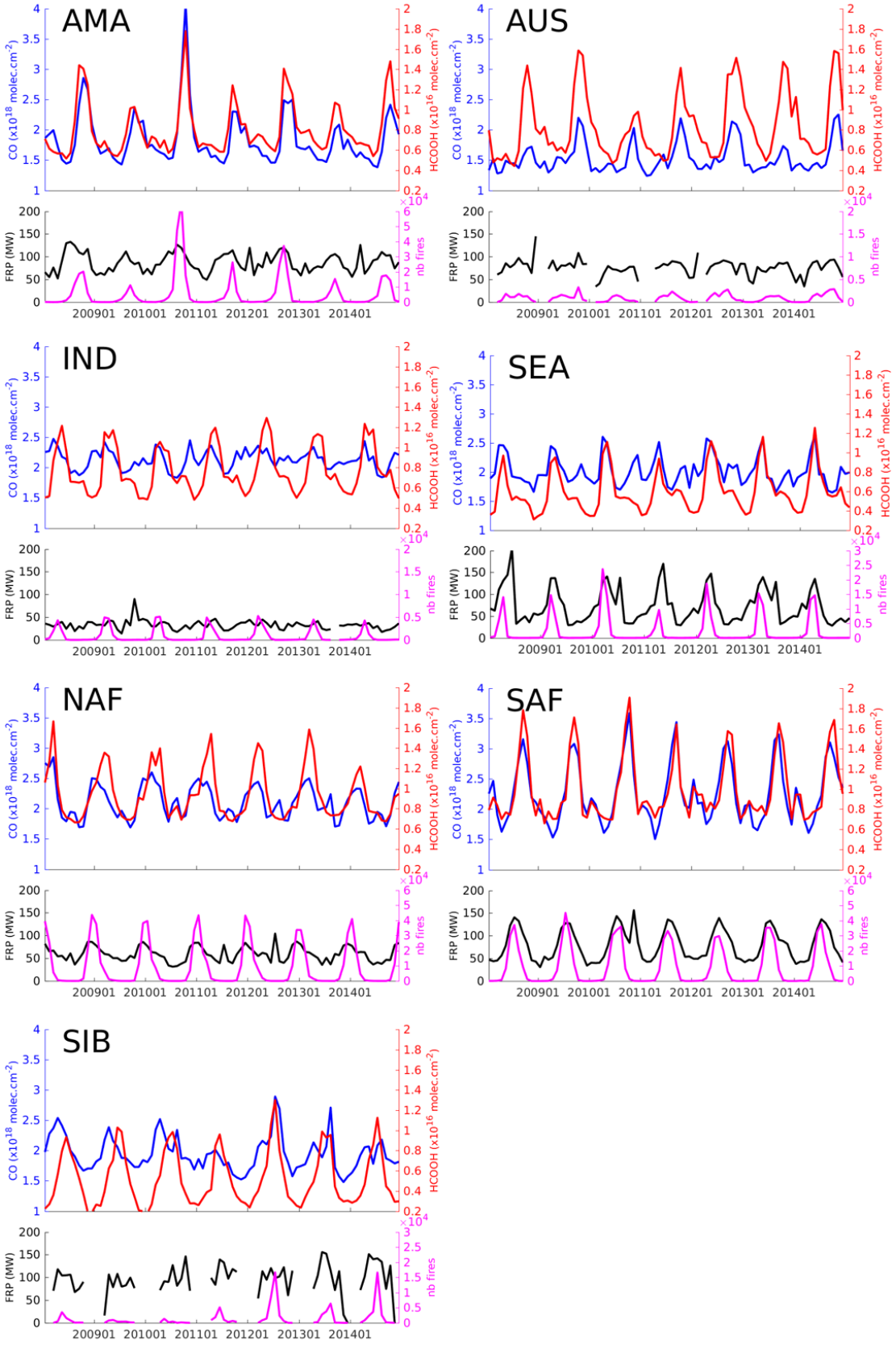

Figure 2: Time-series from 2008 to 2014 of the monthly means of IASI CO (blue) and HCOOH (red) total columns in 10^{18} molec/cm^2 and in 10^{16} molec/cm^2, respectively, FRP (black) in MegaWatts and the number of fires (magenta) from MODIS over the seven regions (AMA=Amazonia, AUS=Australia, IND = India, SEA = Southern East Asia, NAF= Northern Africa, SAF= Southern Africa, SIB= Siberia).

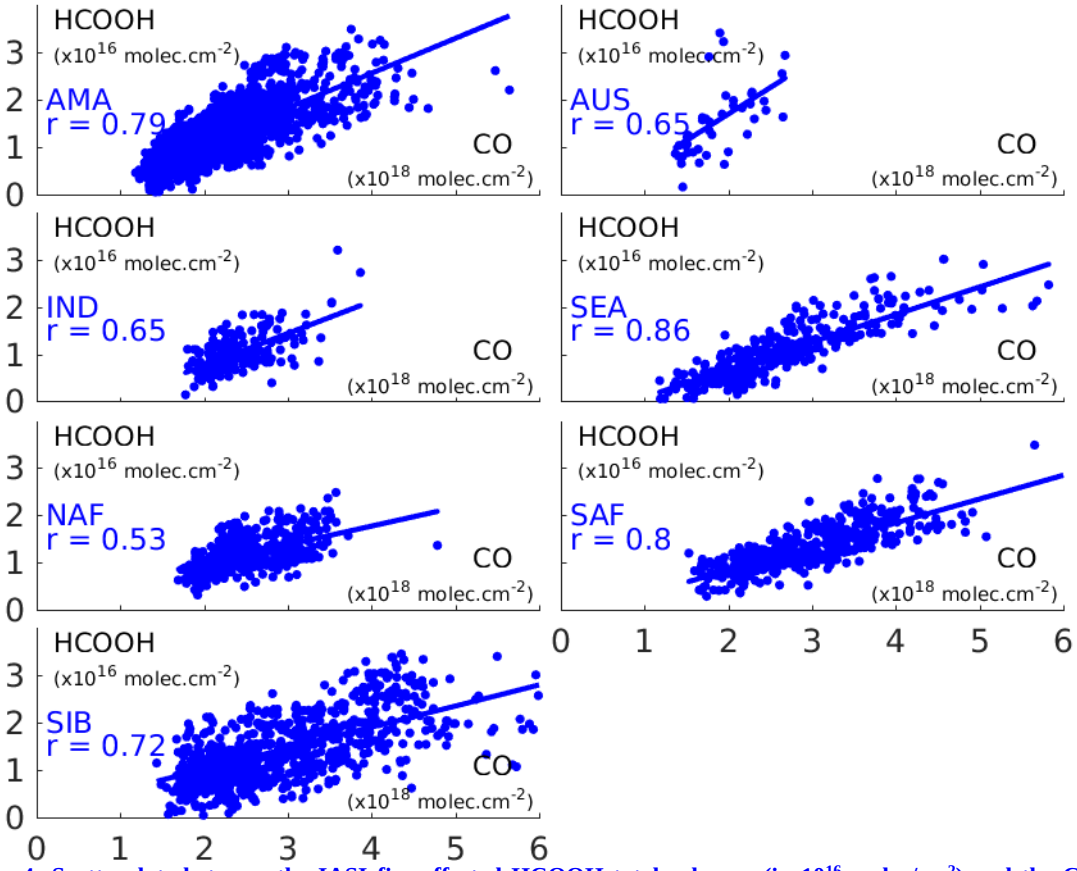

Figure 4: Scatterplots between the IASI fire-affected HCOOH total columns (in 10^{16} molec/cm^2) and the CO total columns (in 10^{18} molec/cm^2) over the seven regions (AMA=Amazonia, AUS=Australia, IND = India, SEA = Southern East Asia, NAF= Northern Africa, SAF= Southern Africa, SIB= Siberia).The linear regression is represented by the blue line and the correlation coefficient is also provided for each region.

Page 22, Figure 3, caption line 4 – Clarify text describing the percentiles

The sentences "The whiskers encompass values from 25th-1.5×(75th-25th) to the 75th+1.5× (75th-25th). This range covers more than 99% of a normally distributed data set." Have been changed by:

"The whiskers encompass values from 25^{th}-1.5×(75^{th}-25^{th}) to the 75^{th}+1.5× (75^{th}-25^{th}). This range of values corresponds to approximately 99.3% coverage if the data are normally distributed. "

Determination of enhancement ratios of HCOOH relative to CO in biomass burning plumes by the Infrared Atmospheric Sounding Interferometer (IASI)

Matthieu Pommier[1,*], Cathy Clerbaux[1,2], Pierre-Francois Coheur[2]

1 LATMOS/IPSL, UPMC Univ. Paris 06 Sorbonne Universités, UVSQ, CNRS, Paris, France
2 Spectroscopie de l'Atmosphère, Chimie Quantique et Photophysique, Université Libre de Bruxelles (ULB), Brussels, Belgium
*now at: Norwegian Meteorological Institute, Oslo, Norway

Correspondence to: Matthieu Pommier (matthieup@met.no)

Abstract. Formic acid (HCOOH) concentrations are often underestimated by models and its chemistry is highly uncertain. HCOOH is, however, among the most abundant atmospheric volatile organic compounds and it is potentially responsible for rain acidity in remote areas. HCOOH data from the Infrared Atmospheric Sounding Interferometer (IASI) are analyzed from 2008 to 2014, to estimate enhancement ratios from biomass burning emissions over seven regions. Fire-affected HCOOH and CO total columns are defined by combining total columns from IASI, geographic location of the fires from MODerate resolution Imaging Spectroradiometer (MODIS), and the surface wind speed field from the European Centre for Medium-Range Weather Forecasts (ECMWF). Robust correlations are found between these fire-affected HCOOH and CO total columns over the selected biomass burning regions, allowing the calculation of enhancement ratios equal to $7.30\times10^{-3}\pm0.08\times10^{-3}$ mol/mol over Amazonia, $11.10\times10^{-3}\pm1.37\times10^{-3}$ mol/mol over Australia, $6.80\times10^{-3}\pm0.44\times10^{-3}$ mol/mol over India, $5.80\times10^{-3}\pm0.15\times10^{-3}$ mol/mol over Southern East Asia, $4.00\times10^{-3}\pm0.19\times10^{-3}$ mol/mol over Northern Africa, $5.00\times10^{-3}\pm0.13\times10^{-3}$ mol/mol over Southern Africa, and $4.40\times10^{-3}\pm0.09\times10^{-3}$ mol/mol over Siberia, in a fair agreement with previous studies. In comparison with referenced emission ratios, it is also shown that the selected agricultural burning plumes captured by IASI over India and Southern East Asia correspond to recent plumes where the chemistry or the sink does not occur. An additional classification of the enhancement ratios by type of fuel burned is also provided, showing a diverse origin of the plumes sampled by IASI, especially over Amazonia and Siberia. The variability in the enhancement ratios by biome over the different regions show that the levels of HCOOH and CO do not only depend on the fuel types.

1. Introduction

Formic acid (HCOOH) is one of the most abundant carboxylic acids present in the atmosphere. HCOOH is mainly removed from the troposphere through wet and dry deposition, and to a lesser extent by the OH radical. It is a relatively short-lived species with an average lifetime in the troposphere of 3–4 days (Paulot et al., 2011; Stavrakou et al., 2012). HCOOH contributes a large fraction to acidity in precipitation in remote areas (e.g. Andreae et al., 1988).

HCOOH is mainly a secondary product from other organic precursors. The largest global source of HCOOH is biogenic and follows the emissions of isoprene, monoterpenes, other terminal alkenes (e.g., Neeb et al., 1997; Lee et al., 2006; Paulot et al., 2011), alkynes (Hatakeyama et al., 1986; Bohn et al., 1996), and acetaldehyde (Andrews et al., 2012; Clubb et al., 2012). There are also small direct emissions by vegetation (Keene and Galloway, 1984, 1988; Gabriel et al., 1999) and biomass burning (e.g. Goode et al., 2000). Other studies highlighted the existence of other sources, such as from ants (Graedel and Eisner, 1988), dry savanna soils (Sanhueza and Andreae, 1991), motor vehicles (Kawamura et al., 1985; Grosjean, 1989), abiological formation on rock surfaces (Ohta et al., 2000) and cloud processing (Chameides et al., 1983). Their contributions are very uncertain and most are probably minor.

More generally there are still large uncertainties on the sources and sinks of HCOOH, and on the relative contribution of anthropogenic and natural sources, despite the fact that recent progress has been made possible by using the synergy between atmospheric models and satellite data (e.g. Stavrakou et al., 2012; Chaliyakunnel et al., 2016). These uncertainties have an impact on our understanding of the HCOOH tropospheric chemistry, as on the oxidizing capacity of the atmosphere (i.e. the chemistry of OH in cloud water - Jacob, 1986; the heterogeneous oxidation of organic aerosols - Paulot et al., 2011) or the origin of the acid rains. One of the large uncertainties in the HCOOH tropospheric budget seems to be the underestimation of the emissions from forest fires, as recently suggested by Stavrakou et al. (2012), Cady-Pereira et al. (2014) and Chaliyakunnel et al (2016).

One way to estimate the atmospheric emissions of pyrogenic species is the use of emission factors. The emission factors are often obtained from ground and airborne measurements or from small fires burned under controlled laboratory conditions. The emission factors can also be derived from enhancement ratios of the target species relative to a reference species, which is often carbon monoxide (CO) or carbon dioxide (CO_2) due to their long lifetime (e.g. Hurst et al., 1994) and are based on the characteristic of the combustible and hence depend on the type of biomass burning. However, the difference between an emission ratio and an enhancement ratio is that emission ratios are calculated from measurements at the time of emission and enhancement ratios are related to the ongoing chemistry. To correctly convert these enhancement ratios to emission ratios, the decay of the chemical species need to be taken into account or assumptions need to be made, suggesting that the enhancement ratios are equivalent to emission ratios, hence measured at the source and not impacted by chemistry.

Compilations of numerous enhancements ratios, emission ratios and emission factors for several trace gases from measurements at various locations world-wide are published regularly (e.g. Akagi et al., 2011) in order to facilitate their use in Chemistry Transport Models.

There has been a recent interest in calculating enhancement ratios and emission factors from satellite data (e.g. Rinsland et al., 2007; Coheur et al., 2009; Tereszchuk et al., 2011). The above difficulty of inferring emission factors using the satellite observations comes from the fact that these observations are indeed typically made in the free/upper troposphere and further downwind of the fires. The fact that satellite mainly probe transported plumes where chemistry modifies the original composition explains why the use of enhancement ratio is more relevant than emission ratio.

Only a few papers have reported on the use of satellite retrievals to study tropospheric HCOOH including the nadir-viewing Infrared Atmospheric Sounding Interferometer (IASI) (e.g. Razavi et al., 2011; Stavrakou et al., 2012; R'Honi et al., 2013; Pommier et al., 2016), and Tropospheric Emission Spectrometer (TES) (e.g. Cady-Pereira et al., 2014; Chaliyakunnel et al., 2016). Other studies have used the solar occultation Atmospheric Chemistry Experiment – Fourier Transform Spectrometer (ACE-FTS) which measures the atmospheric composition in the upper troposphere (e.g. Rinsland et al., 2006; Gonzalez Abad et al., 2009; Tereszchuk et al., 2011; 2013) and the Michelson Interferometer for Passive Atmospheric Sounding (MIPAS) limb instrument, which is sensitive to around 10 km (Grutter et al., 2010).

These Infrared (IR) sounders have limited vertical sensitivity as compared to ground-based or airborne measurements but their spatial coverage represents a major advantage, which allows observation of remote regions which are sparsely studied by field measurements, like the biomass burning regions.

This work aims to provide a list of enhancement ratios of HCOOH relative to CO over several biomass burning regions. For this, we analyzed seven years of IASI measurements, between 2008 and 2014. Section 2 describes the IASI satellite mission and the retrieval characteristics for the CO and the HCOOH total columns. Section 3 presents the fire product used from the MODerate resolution Imaging Spectroradiometer (MODIS) to identify the fire locations. Section 4 details the methodology used to identify of the IASI fire-affected observations. In Section 5 we describe and analyze the enhancements ratios obtained from the IASI measurements, including an analysis of these ratios by type of fuel burned and we compare these values to those available in the literature. Finally, the conclusions are presented in Section 6.

2. HCOOH and CO columns from IASI

2.1 The IASI mission

IASI is a nadir-viewing Fourier Transform Spectrometer. Two models are currently in orbit. The first model (IASI-A), was launched onboard the METOP-A platform in October 2006. The second instrument was launched in September 2012 onboard METOP-B. Owing to its wide swath, IASI delivers near global coverage twice a day with observation at around 09:30 and 21:30 local time. Each atmospheric view is composed of 2×2 circular pixels with a 12 km footprint diameter, spaced out by 50 km at nadir. IASI measures in the thermal infrared part of the spectrum, between 645 and 2760 cm^{-1}. It records radiance from the Earth's surface and the atmosphere with an apodized spectral resolution of 0.5 cm^{-1}, spectrally sampled at 0.25 cm^{-1}. IASI has a wavenumber-dependent radiometric noise ranging from 0.1 to 0.4 K for a reference blackbody at 280 K (Clerbaux et al., 2009), and more specifically around 0.15 K for HCOOH and 0.20 K for the CO spectral ranges (~1105 cm^{-1} and ~2150 cm^{-1}, respectively).

The HCOOH and CO columns from IASI are used hereafter to determine the enhancement ratios of HCOOH. CO is chosen as reference due to its longer tropospheric lifetime (a few weeks to a few months depending on latitude and time of year) as compared to HCOOH. In our study we use CO as the reference and not CO_2 since variations in CO_2 concentration are difficult to measure with sufficient accuracy from IASI (Crevoisier et al., 2009).

2.2 The CO retrieval characteristics

The CO concentrations are retrieved from IASI using the FORLI-CO software (Hurtmans et al., 2012), which uses an optimal estimation method based on Rodgers (2000). The spectral range used for the retrieval is between 2143 and 2181.25 cm^{-1}. The CO total columns have been validated for different locations and atmospheric conditions (e.g. De Wachter et al., 2012; Kerzenmacher et al., 2012) and the comparison with other data have shown good overall agreement, even if some discrepancies were found within CO-enriched plumes (reaching 12% over the Arctic in summer, see Pommier et al., 2010; and reaching 17% in comparison with other IR sounders, see George et al., 2009). These data were also used previously to study biomass burning plumes (e.g. Turquety et al., 2009; Pommier et al., 2010; Krol et al., 2013; Whitburn et al., 2015).

In order to keep only the most reliable retrievals, the selected data used have a root-mean-square error lower than 2.7×10^{-9} $W/(cm^2\ cm^{-1}\ sr)$ and a bias ranging between -0.15 and 0.25×10^{-9} as recommended in Hurtmans et al. (2012).

2.3 The HCOOH retrieval characteristics

The retrieval is based on the determination of the brightness temperature difference (ΔT_b) between spectral channels with and without the signature of HCOOH. The reference channels used for the calculation of ΔT_b were chosen on both sides of the HCOOH Q-branch (1105 cm^{-1}), i.e., at 1103.0 and 1109.0 cm^{-1}. These ΔT_b were converted into total columns of HCOOH using conversion factors compiled in look-up tables. This simple and efficient retrieval method is described in more detail in Pommier et al. (2016).

As shown in Pommier et al. (2016), the vertical sensitivity of the IASI HCOOH total column ranges between 1 and 6 km. That study also showed that large HCOOH total columns were detected over biomass burning regions (e.g. Africa, Siberia) even if the largest values were found to be underestimated. This underestimation, which is less than 35% for the columns smaller than 2.5×10^{16} $molec/cm^2$ (Pommier et al., 2016), will affect the enhancement ratios calculated in this work.

On the other hand, a large overestimation of the IASI HCOOH columns was shown in comparison with ground-based FTIR. This overestimation was larger for background columns (expected to reach 80% for a column close to 0.3×10^{16} $molec/cm^2$), which can also impact our enhancement ratios.

3. MODIS

To identify the fire locations (hotspots), the fire product from MODIS on board the polar orbiting sun-synchronous NASA Terra and Aqua satellites (Justice et al., 2002; Giglio et al., 2006) are used. The Terra and Aqua satellites equatorial overpass times are ~10:30 (am and pm) and ~01:30 (am and pm) local time, respectively. Fire pixels are 1 km×1 km in size at nadir.

For this work, we more specifically use the Global Monthly Fire Location Product (MCD14ML, Level 2, Collection 5) developed by the University of Maryland (https://earthdata.nasa.gov/data/near-real-time-data/firms/active-fire-data#tab-content-6) which, for each detected fire pixel, includes the geographic location of the fire, the fire radiative power (FRP), the confidence in detection, and the acquisition date and time. The FRP provides a measure of fire intensity that is linked to the fire fuel consumption rate (e.g. Wooster et al., 2005). Only data presenting a high confidence percentage are used, i.e. higher than or equal to 80% as recommended in the MODIS user's guide (Giglio, 2013).

To characterize each MODIS hotspot by the type of fuel burned, the Global Mosaics of the standard MODIS land cover type data product (MCD12Q1) in the IGBP Land Cover Type Classification (Friedl et al., 2010; Channan et al., 2014) with a 0.5° × 0.5° horizontal resolution has also been used (http://glcf.umd.edu/data/lc/). As the annual variability in this product is limited (not shown) and since the period available (from 2001 to 2012) does not fully match the period of the IASI mission, only the data for 2012 have been used. Whitburn et al. (2017) have also used this MCD12Q1 product to determine their IASI-derived NH_3 enhancement ratios by vegetation types.

4. Identifying fire-affected IASI observations

4.1 The selected areas

The determination of the biomass burning regions is based on the MODIS fire product. Figure 1 highlights the main areas that contributed to the biomass burning for the period between 2008 and 2014. Seven regions were selected for this work: Amazonia (AMA, 5-15°S 40-60°W), corresponding mainly to the Brazilian Cerrado, Australia (AUS, 12-15°S 131-135°E), Northern Africa (NAF, 3-10°N 15-30°E), Southern Africa (SAF, 5-10°S 15-30°E), Southern East Asia (SEA, 18-27°N 96-105°E), India (IND, 15-27°N 75-88°E) and Siberia (SIB, 55-65°N 80-120°E). Among these regions, India and Siberia do not represent the most active regions in terms of number of fires. It seemed however important to also investigate them. One first reason for this is that Pommier et al. (2016) showed a misrepresentation of the fire emissions of HCOOH over India. Secondly, India also encounters excess of acidity in rainwater, which could be partly attributed to biomass burning (e.g. Bisht et al., 2014). Concerning Siberia, this region and the surrounding areas experienced intense fires over some years, such as during the summer 2010 (Pommier et al., 2016; and R'honi et al. 2013 for the region close to Moscow). The classification of the vegetation from the MODIS product has also been used for a detailed analysis of the enhancement ratios for these regions (Fig. 1).

4.2 The IASI data used

For this work, both the daytime and nighttime IASI data were used. We have verified that using only the daytime retrievals did not change the results. Figure 2 presents the time-series of the monthly mean for the HCOOH and CO total columns over the seven selected regions. The number of fires and their FRP are also indicated. The variation in the total columns of HCOOH and CO matches relatively well with the variation of the number of fires. It is also worth noting that these variations in the total columns do not depend on the intensity of the fires as shown by Fig. 2 and by the scatterplots with the values characterizing each fire as described below (not shown).

The monthly HCOOH and CO total columns are found to be highly correlated over the selected biomass burning regions (correlation coefficient, r, from 0.75 to 0.91), except over India (r=0.34) and Siberia (r=0.58). Over both regions, the impact of sources other than biomass burning is thus not negligible. Over India, the CO budget is influenced by long-range transport (e.g. Srinivas et al., 2016) and the anthropogenic emissions also have a large impact (e.g. Ohara et al., 2007). This could explain why the variation in CO does not follow perfectly the variation in the number of fires and that the difference between the

background level and the CO peaks is less marked than for the HCOOH. Over Siberia, a temporal shift between the highest peaks for CO and for HCOOH is noticed for some years, such as for 2009, 2010 and 2011. For these years, the variation in CO does not follow the variation in the number of fires. The large region selected over Siberia is known also to be impacted by CO-enriched plumes transported from other regions, such as polluted air masses from China (e.g. Paris et al., 2008) or from Europe (e.g. Pochanart et al., 2003). These external influences interfere with the CO plumes originating from forest fires measured over this region.

Despite the overall good match between the number of fires and the variation in HCOOH and CO, we are not certain that the HCOOH and the CO were emitted solely by fires, and the discrimination between a natural and an anthropogenic origin for each compound is challenging. This assessment is particularly obvious for IND and SIB. To isolate the HCOOH and CO signals measured by IASI, potentially emitted by a fire, we decided to only use the data in the vicinity of each MODIS hotspot. To do so, we co-located the IASI data at 50 km around each MODIS pixel and between 0 and 5h from the time registered by MODIS for each detected fire, so that each MODIS pixel is associated with a mean value of HCOOH and CO total columns from IASI.

With these co-location criteria, good correlation coefficients, calculated by linear least-square fitting, are found between the HCOOH and CO total columns as shown in Table 1 (upper row). The smaller correlation coefficients, i.e., less than 0.7, are found for India, Australia, Siberia and Northern Africa. It is also important to note that the HCOOH and CO columns are better correlated for India and Siberia compared to the monthly time-series shown in Fig. 2. The three other regions present a large correlation, around 0.8. The high correlation suggests that IASI sampled the same biomass burning air mass for these compounds.

4.3 Importance of the meteorological conditions

As shown in earlier studies, the wind speed can have a large influence on the detection of tropospheric plumes of trace gases from space (e.g NO_2: Beirle et al., 2011; CO: Pommier et al., 2013; SO_2: Fioletov et al., 2015). We have chosen to assign a surface wind speed value for each MODIS hotspot. These meteorological fields were taken from the ECMWF (European Centre for Medium-Range Weather Forecasts) reanalysis data (http://data-portal.ecmwf.int/data/d/interim_full_daily) (Dee et al., 2011). The horizontal resolution of these fields is 0.125° on longitude and latitude with a 6h time step. As shown in Fig 3, the three regions where the HCOOH:CO correlations are found to be high (r close to 0.8), correspond to the regions where the surface wind speed was lower, i.e. for AMA, SEA and SAF. IND has also a low mean and median surface wind speed but the distribution of this surface wind speed over IND is more spread out than for AMA, SEA and SAF. It is also noteworthy that the IND and SEA regions are both characterized by higher wind speed at higher altitudes, i.e. for the pressure levels 650 and 450 hPa (not shown). This shows that the wind speed at higher altitudes has a lower influence on our correlations than the surface wind. When filtering out the data associated with a large surface wind (higher than 1.44 m/s), new correlations between the HCOOH and the CO total columns from IASI are calculated (Table 1 – lower row). This value of 1.44 m/s for the surface wind speed corresponds to the 25th percentile of the distribution of the three regions characterized by the lowest surface wind speed (Fig. 3).

The correlation coefficients, shown on the scatterplots in Fig. 4 and summarized in Table 1 (lower row), increase for all regions except over NAF, where the coefficient is found to be slightly lower than the previous correlation (Table 1 – upper row). The correlation coefficient is significantly improved over IND and SIB (Table 1 – lower row). These results confirm a robust correlation between the HCOOH and the CO total columns measured by IASI in the vicinity of each MODIS fire location.

5. Analysis of the data over the fire regions

5.1. Determination of the enhancement ratios

5.1.1 General analysis

Based on scatterplots in Fig. 4, an enhancement ratio can be calculated for each region. These enhancement ratios defined as $ER_{(HCOOH/CO)}$, correspond to the value of the slope ∂[HCOOH]/∂[CO] found in Fig 4. This technique to determine the $ER_{(HCOOH/CO)}$ is more reliable than using only the columns themselves, i.e. by estimating an $ER_{(HCOOH/CO)}$ for each measurement pair (HCOOH, CO). Indeed, to perform scatterplots helps to identify a common origin for HCOOH and CO. The values of the $ER_{(HCOOH/CO)}$ over each region are summarized in Table 2.

It is known that trace gas concentrations within smoke plumes can vary rapidly with time and are very sensitive to chemistry, so a comparison with previous work is always challenging, especially if these studies were performed over another altitude range, at a different location or period of the year.

A good agreement is however generally found with previous studies, even if it is important to keep in mind that an underestimation of our $ER_{(HCOOH/CO)}$ is possible due to the underestimation in the highest values of HCOOH as over the forest fires (see Section 2.3). On the other hand, the overestimation in the background column can also impact the calculation of our $ER_{(HCOOH/CO)}$. The effects of both biases are, however, limited since most of HCOOH total columns used in our analysis over the selected regions are higher than 0.3×10^{16} molec/cm^2 and lower than 2.5×10^{16} molec/cm^2 as explained in Section 2.3.

Nevertheless, in order to investigate the possible impact of the overestimation in the lower columns and the underestimation in the higher columns on the calculated ratios, a test was performed, by using only HCOOH columns with a thermal contrast larger than 10K. Indeed, the increase in the thermal contrast (i.e. the temperature difference between the surface and the first layer in the retrieved profile) leads to reducing the detection limit as shown in Pommier al. (2016). This enhancement of the detection level helps to minimize the bias in the retrieved total columns as explained in Crevoisier et al. (2014). For the analysis performed here, similar slopes and correlation coefficients were generally calculated, suggesting a negligible effect of this parameter on the biases. The only exception is an increase in $ER_{(HCOOH/CO)}$ over Siberia ($6.5\times10^{-3} \pm 0.19\times10^{-3}$ mol/mol when using only IASI measurements with TC above 10K against 4.4×10^{-3} mol/mol $\pm 0.09\times10^{-3}$ in Table 2). It is worth noting that only 48% of the selected scenes remain over Siberia when applying this filter on thermal contrast (60% for SEA, 77% for AMA, 80% for SAF, 83% for AUS and NAF, and 89% for IND). This implies that the statistics on the fire emissions in the higher latitudes of Siberia is dominated by measurements with a low thermal contrast and thus with HCOOH total columns with higher uncertainties. However, the limited changes in slopes and correlation coefficients give us confidence that the results presented in Table 2 are representative.

5.1.2 Analysis over each region

A few backward trajectories (along 5 days, not shown) have been calculated for our hotspots with the online version of the HYSPLIT atmospheric transport and dispersion modeling system (Rolph, 2017). These trajectories, initialized at different altitudes, confirm a main origin close to the surface of our IASI fire-affected columns. It is however impossible to properly compare the origin of the air masses with previous studies as our studied period (2008-2014) or our studied fires do not necessarily match with plumes described in other publications. It is also difficult to estimate the age of our studied air masses by gathering the plumes during a 7-yr period and without an accurate knowledge of the altitude of the plumes.

When compared with other studies, the best agreement for the values presented in Table 2 is found over Southern Africa where the $ER_{(HCOOH/CO)}$ ($5\times10^{-3} \pm 0.13\times10^{-3}$ mol/mol) is similar to the value calculated by Vigouroux et al. (2012) and Coheur et al. (2007). It also agrees with the broad range of values of emission ratios ($EmR_{(HCOOH/CO)}$) referenced by Sinha et al. (2003). This result corroborates the relevance of the methodology used in this work over this region for the identification of fire-affected IASI columns close to the source. Vigouroux et al. (2012) sampled biomass burning outflow of Southern Africa, Coheur et al. (2007) calculated their $ER_{(HCOOH/CO)}$ in plumes observed over Tanzania in the upper troposphere while Sinha et al. (2003) did it within plumes over Zambia at the origin of the fire.

A few assumptions are needed in order to interpret our $ER_{(HCOOH/CO)}$ but the analysis given hereafter is only indicative since these previous studies did not measure the same plume as those presented in this work. Our $ER_{(HCOOH/CO)}$ is also calculated without making any distinction on the seasonal variation or on the type of biomass burning plumes sampled (e.g. emitted by a savanna fire or by a forest fire). The analysis by biome is presented in Section 5.2. Since these $ER_{(HCOOH/CO)}$ from previous studies and the $EmR_{(HCOOH/CO)}$ from Sinha et al. (2003) agree with our $ER_{(HCOOH/CO)}$, and since HCOOH has a short lifetime, this may suggest that the selected plumes measured by IASI from 2008 to 2014 and those sampled by Vigouroux et al. (2012) and Coheur et al. (2007), encountered a limited secondary production or a low sink (deposition or reaction with OH in the troposphere during their transport). To quantify the role of the chemistry or of the deposition within the plumes, a modeling work should be performed. This is however beyond the scope of this paper.

Another important point is that the decay of HCOOH is faster than for CO. As our $ER_{(HCOOH/CO)}$ is similar to the $ER_{(HCOOH/CO)}$ from the other studies and to the $EmR_{(HCOOH/CO)}$ given in Sinha et al. (2003), this could suggest that all these plumes (from our study, from Vigouroux et al. (2012) and Coheur et al. (2007)) are rapidly advected in the troposphere. Our $ER_{(HCOOH/CO)}$ differs however from the value in Rinsland et al. (2006) ($11.3\times10^{-3} \pm 7.6\times10^{-3}$ mol/mol), since our ratio is 55% lower. One possible explanation is the multi-origin of the plumes studied by Rinsland et al. (2006), since, based on their backward trajectories, their plumes could be influenced by biomass burning originating from Southern Africa and/or from Southern America. The travel during the few days across the Atlantic Ocean may explain the change in their $ER_{(HCOOH/CO)}$.

It is worth noting that the ACE-FTS instrument used in their study works in a limb solar occultation mode. This means that the atmospheric density sampled by the instrument is larger than the one measured by the nadir geometry with IASI. However, the difference in geometry cannot explain why we find an agreement with the ACE-FTS measurements values reported by Coheur et al. (2007) and a disagreement with those from Rinsland et al. (2006). Part of the difference could be associated with the difference in the assumptions used in both retrievals (e.g. the a priori).

The $ER_{(HCOOH/CO)}$ from our work is also 15% lower than the $EmR_{(HCOOH/CO)}$ in Yokelson et al. (2003) ($5.9\times10^{-3} \pm 2.2\times10^{-3}$ mol/mol) who calculated their value within plumes over Zambia, Zimbabwe and South Africa. With this difference we can also suggest the presence of a sink of HCOOH within the plumes detected by IASI, or that this slight underestimation is simply related to the faster decay of HCOOH than the one of CO. Conversely, the $ER_{(HCOOH/CO)}$ retrieved from IASI is twice that of Chaliyakunnel et al. (2016) ($2.6\times10^{-3} \pm 0.3\times10^{-3}$ mol/mol). Chaliyakunnel et al. (2016) developed an approach allowing the determination of pyrogenic $ER_{(HCOOH/CO)}$ by reducing the impact of the mix with the ambient air. To do so, they calculated the $ER_{(HCOOH/CO)}$ in the vicinity of fire count from MODIS (averaged in a cell having the resolution of the GEOS-Chem model, i.e. 2°× 2.5°) and they differentiated this value with a background $ER_{(HCOOH/CO)}$ defined by the concentrations distant from these fires. They concluded that their most reliable value on the amount of HCOOH produced from fire emissions was obtained for African fires.

Over Northern Africa, the calculated $ER_{(HCOOH/CO)}$ ($4\times10^{-3} \pm 0.19\times10^{-3}$ mol/mol) is 42% higher than the $ER_{(HCOOH/CO)}$ calculated in Chaliyakunnel et al. (2016) ($2.8\times10^{-3} \pm 0.4\times10^{-3}$ mol/mol). It is worth noting that NAF is the region characterized by a scatterplot with the lowest correlation coefficient (Fig. 4).

A larger difference is found over Australia where the $ER_{(HCOOH/CO)}$ is $11.1\times10^{-3} \pm 1.37\times10^{-3}$ mol/mol. This $ER_{(HCOOH/CO)}$ is roughly the mean of both values reported by Paton-Walsh et al. (2005) and Chaliyakunnel et al. (2016). The difference between our work and that of Paton-Walsh (2005) may be explained by the different origin of the probed plume. In our case, the studied area corresponds to the Northern part of the Northern Territory with savanna-type vegetation (as shown in Section 5.2) while Paton-Walsh et al. (2005) sampled bush fire plumes coming from the Eastern Coast of Australia, representative of Australian temperate forest. In the work done by Chaliyakunnel et al. (2016), a quite uncertain value is reported ($4.5\times10^{-3} \pm 5.1\times10^{-3}$ mol/mol), with an error larger than their $ER_{(HCOOH/CO)}$.

Over Amazonia, our $ER_{(HCOOH/CO)}$ ($7.3\times10^{-3} \pm 0.08\times10^{-3}$ mol/mol) is similar to the value given in Chaliyakunnel et al. (2016), who report, however, a larger bias over Amazonia. Over this region, our $ER_{(HCOOH/CO)}$ is higher than the one obtained by

González Abad et al. (2009) with ACE-FTS in the upper troposphere ($5.1\times10^{-3} \pm 1.5\times10^{-3}$ mol/mol). This difference with the study done by González Abad et al. (2009) may be explained by the difference in the altitude of the detection of the forest fire plume between IASI (mid-troposphere) and ACE-FTS (upper-troposphere) and thus by a difference in the ongoing chemistry within their respective sampled plumes. The geometry of the sampling (nadir vs limb) or the difference in the retrieval may also have an impact in the retrieved HCOOH.

The Siberian $ER_{(HCOOH/CO)}$ (4.4×10^{-3} mol/mol $\pm$ 0.09×10^{-3}) is found to be in good agreement with the wide range of values obtained by Tereszchuk et al. (2013) and Viatte et al. (2015). This $ER_{(HCOOH/CO)}$ is however lower than the ratios calculated by R'Honi et al. (2013) who focused on the extreme fire event that occurred in 2010.

For India and Southern East Asia, a comparison is not possible since no previous studies were reported. The comparison is performed next, based on the emission factors.

5.2. Analysis based on the type of vegetation

We have complemented our comparison of the enhancement ratios by comparing our ratios to emissions ratios calculated from emission factors found in literature. The main argument to perform such comparison is the lack of measurements of enhancement ratios over IND and SEA. Furthermore, such comparison from emission factors facilitates an analysis based on hypothesis about the type of vegetation burned.

Even if our methodology attempts to characterize the HCOOH emitted by biomass burning close to the source, our columns are probably not representative of the emission at the origin of the fire. The altitude of the sampling (mid-troposphere), even if an influence from the surface is shown, and the age of the plumes (at least a few hours) have a large impact on our enhancement ratios.

To perform a proper comparison with emission ratios, our enhancement ratios should be converted to emission ratios. To do so, it would be essential to take into account the decay of the compounds during the transport of the plume. However, due to the methodology used, i.e. averaging the data collected during a few hours (between 0 and 5h from the time registered by MODIS for each detected fire), the calculation of the decay of each compound is not possible. We therefore have compared our enhancement ratios to emission ratios and the comparison presented hereafter is mostly illustrative.

For both IND and SEA regions, the emission ratios have been calculated from the emission factors provided in Akagi et al. (2011). For the other regions, in addition to the values from Akagi et al. (2011), emission ratios were similarly calculated from emission factors given in other studies (listed in Table 3).

Based on the emission ratios, the emission factors are usually derived by this following Equation:

$$EF_{HCOOH} = EF_{CO} \times MW_{HCOOH}/MW_{CO} \times EmR_{(HCOOH/CO)} \quad (1)$$

EF_{HCOOH} is the emission factor for HCOOH; $EmR_{(HCOOH/CO)}$ is the molar emission ratio of HCOOH with respect to CO; MW_{HCOOH} is the molecular weight of HCOOH; MW_{CO} is the molecular weight of CO and EF_{CO} is the emission factor for CO for dry matter, set to the value taken from Akagi et al. (2011).

Thus, based on equation (1), $EmR_{(HCOOH/CO)}$ values were calculated and compared with our $ER_{(HCOOH/CO)}$ (Table 3). In this calculation, the vegetation type characterizing each region is important. Some regions are composed of a mix of vegetation types as shown in Fig. 1. This is for example the case for AMA and SAF (e.g. White, 1981). Thus following the classification from Akagi et al. (2011), AMA and SAF are composed of tropical forest and savanna, characterized by an EF_{CO} of 93±27 g/kg and 63±17 g/kg, respectively (Akagi et al., 2011). AUS and NAF correspond to a savanna fuel type. SIB is a boreal forest area with an EF_{CO} of 127±45 g/kg. Based also on the maps shown by Fig. 9 in Schreier et al. (2014), Fig. 13 in van der Werf, et al. (2010), the soil for IND is supposed to be mainly composed of cropland (agriculture), which is associated to an EF_{CO} of 102±33 g/kg, and probably also by extratropical forest which is characterized by an EF_{CO} equal to 122±44 g/kg and savanna with an EF_{CO} of 63±17 g/kg. The fuel type for SEA is supposed to be a mix of extratropical forest and savanna, with an EF_{CO} of 122±44

g/kg, and 63±17 g/kg, respectively. Cropland fuel type was also used since large agricultural biomass burning is occurring in this region (e.g. Duc et al., 2016).

In addition to the $EmR_{(HCOOH/CO)}$ calculated from the EF_{HCOOH} given in the literature, a classification for our $ER_{(HCOOH/CO)}$ has also been done, based on the data from the MCD12Q1 product. As each hotspot is associated with a land cover value defined by the MCD12Q1 product, enhancement ratios by biome have been calculated. The limitations of this dataset are its coarse resolution (0.5° × 0.5°) and the lack of seasonal variation. It gives however a supplementary information on the type of fuel burned identified by MODIS. The corresponding $ER_{(HCOOH/CO)}$ are provided in Table 3. Only the values calculated from a scatterplot with a correlation coefficient higher than 0.4 are reported.

Despite the assumptions made, a fair agreement is found over Southern Africa. Our $ER_{(HCOOH/CO)}$ ($5\times10^{-3} \pm 0.13\times10^{-3}$ mol/mol) is indeed similar to the $EmR_{(HCOOH/CO)}$ calculated from Sinha et al. (2004) by using savanna fuel type, and the $ER_{(HCOOH/CO)}$ is between both values calculated from Yokelson et al. (2003). This agreement is consistent since both previous studies sampled plumes emitted by savanna fires. Yokelson et al. (2003) and Sinha et al. (2004) both used the same sampling strategy. They sampled fire plumes by penetrating several minutes old plumes at relatively low altitude (up to 1.3 km for Sinha et al. (2004) and just above the flame front for Yokelson et al. (2003)). This agreement shows, as already described in the previous section, that our $ER_{(HCOOH/CO)}$ over Southern Africa is similar to their $EmR_{(HCOOH/CO)}$. It is also noteworthy, based on the MODIS land cover type product, that all the studied hotspots are defined as savanna fires. On other hand, our $ER_{(HCOOH/CO)}$ is also similar to the $EmR_{(HCOOH/CO)}$ from Akagi et al. (2011) but for the tropical forest. A large underestimation compared to Rinsland et al. (2006) is found. This underestimation confirms the disagreement with their study already shown in Table 2.

Over Northern Africa, our $ER_{(HCOOH/CO)}$ is twice as large as the $EmR_{(HCOOH/CO)}$ provided by Akagi et al. (2011), probably due to the lower correlation found in our scatterplot. It is highly probable that our presumed fire-affected IASI columns are indeed impacted by other air masses. The land classification based on the MODIS product also shows a diverse origin of the hotspots. For Amazonia, the calculated $ER_{(HCOOH/CO)}$ ($7.3\times10^{-3} \pm 0.08\times10^{-3}$ mol/mol) is close to the $EmR_{(HCOOH/CO)}$ given in Akagi et al. (2011) for the tropical forest (5.2×10^{-3} mol/mol), but it is three times higher than the values derived from Yokelson et al. (2007; 2008) for the same vegetation type. For the latter, it is worth noting that their factors have been corrected a posteriori (scaled down by a factor of 2.1), as described in their comment following the paper done by R'Honi et al. (2013) (see Yokelson et al., 2013). As Yokelson et al. (2007; 2008) sampled the forest fire plumes by penetrating recent columns of smoke 200–1000m above the flame front, our $ER_{(HCOOH/CO)}$ may reflect a secondary production of HCOOH. This assuming secondary production is less substantial in comparison with the value from Akagi et al. (2011). The classification based on the type of fuel burned shows diverse origin of the fire plumes over Amazonia. Six biomes have been identified following the classification from the MCD12Q1 product.

Over Australia and over Siberia, the calculated $ER_{(HCOOH/CO)}$ is overestimated compared to the $EmR_{(HCOOH/CO)}$ given in Akagi et al. (2011) for a savanna fire and for a boreal forest, respectively. If our value for near-source estimation is correct, this would probably mean that the direct emission is underestimated (by 450% over Australia and by 60% over Siberia) or that a large secondary production of HCOOH from Australian and Siberian fires occurred. These hypotheses in biased emissions and/or secondary production need, however, to be verified with modeling studies. Over Australia, the difference is very large even if the comparison done by Pommier al. (2016) with FTIR measurements showed that the lowest bias was found for the Australian site (-2% at Wollongong). Over Siberia, we also note that the region is characterized by fires emitted from six types of biome based on the classification from MODIS.

Finally, in this comparison, the studied plumes over India and Southern East Asia are certainly related to agricultural fires, even if the evergreen broadleaf forest seems to dominate in the MODIS land cover type product. This is strongly possible as agricultural residue burning is prevalent in these regions (e.g. Kaskaoutis et al., 2014; Vadrevu et al., 2015). Over India and over Southern East Asia, our $ER_{(HCOOH/CO)}$ ($6.8\times10^{-3} \pm 0.44\times10^{-3}$ mol/mol for India and $5.8\times10^{-3} \pm 0.15\times10^{-3}$ mol/mol for Southern East Asia) are close to the value referenced by Akagi et al. (2011) for cropland fires (6×10^{-3} mol/mol). Since our

$ER_{(HCOOH/CO)}$ are close to $EmR_{(HCOOH/CO)}$ derived from the EF_{HCOOH} in Akagi et al. (2011), this may suggests that the plumes studied over the 7-yr period correspond to fresh plumes where the chemistry or the physical sink is small. This is further supported by the fact that among the seven regions, IND and SEA have larger vertical velocity means close to the surface indicating a larger rising motion of the air masses (not shown).

In general, the $ER_{(HCOOH/CO)}$ calculated for a specific biome varies with the regions. This shows that the type of vegetation is not the only factor influencing the $ER_{(HCOOH/CO)}$. The ongoing chemistry within a plume is important and the age of the air masses impact the level of HCOOH and CO in the plumes.

6. Conclusions

Seven years of HCOOH data measured by IASI over seven different fire regions around the world were analyzed (AMA = Amazonia, AUS = Australia, IND = India, SEA = Southern East Asia, NAF = Northern Africa, SAF = Southern Africa, SIB = Siberia). By taking into account the surface wind speed and by characterizing each MODIS fire hotspot with a value of HCOOH and CO total columns, this work established enhancement ratios for the seven biomass burning areas and compared them to previously reported values found in literature.

The difficulties in performing such a comparison are associated with the difference in locations, altitude of the sampling and age of each fire plume studied in these previous publications. A fair agreement was however found for the enhancement ratios calculated in this work, in comparison with other studies, using satellite, airborne or FTIR measurements.

In agreement with previous studies, the plumes from Southern African savanna fires may reflect a limited secondary production or a limited sink occurring in the upper layers of the troposphere during their transport. Such assumptions, however, are difficult to verify by comparing individual plumes (from previous studies) with plumes gathered during a 7-yr period (from IASI), and remain speculative without a detailed modeling study. Plumes from agricultural fires over India and Southern East Asia probably correspond to fresh plumes as our $ER_{(HCOOH/CO)}$ based on the 7-yr IASI measurements are similar to the $EmR_{(HCOOH/CO)}$ calculated from emission factors provided by Akagi et al. (2011).

A very good agreement in $ER_{(HCOOH/CO)}$ was found over Amazonia, especially in comparison with the work done by Chaliyakunnel et al. (2016) who determined pyrogenic $ER_{(HCOOH/CO)}$.

Fires over Australia and over Siberia are probably underestimated in terms of direct emission or secondary production of HCOOH. The analysis over Australia is however complicated as our $ER_{(HCOOH/CO)}$ approximately corresponds to the mean of the values reported in Paton-Walsh et al. (2005) and in Chaliyakunnel et al. (2016); and it is also 450% higher than the $EmR_{(HCOOH/CO)}$ derived from Akagi et al. (2011). The underestimation by 60% over Siberia is consistent with conclusions given in R'Honi et al. (2013). The calculation of the $ER_{(HCOOH/CO)}$ by biome shows that Siberian plumes are related to the burning of six different vegetation classes. The underestimation reported is thus difficult to confirm without the use of a chemical transport model.

The values found over Northern Africa were the more difficult to interpret as this region is characterized by a poorer correlation between our fire-affected HCOOH and CO total columns.

Finally, the estimation of the $ER_{(HCOOH/CO)}$ calculated by the type of vegetation burned, as referenced in the MODIS product, varies with the regions. This shows that other parameters than the type of fuel burned also influence the $ER_{(HCOOH/CO)}$.

With these findings and by updating the enhancement ratios, an interesting modeling study could be performed to estimate a new tropospheric budget for HCOOH. This IASI data set may also be used in the future to study a single plume at different times to inform on the loss during transport. Further insight into the transport and chemistry may be gained by using IASI's capability to measure several fire species simultaneously, such as HCN or C_2H_2 (e.g. Duflot et al., 2015). This would be useful for the characterization of the chemistry ongoing in a fire plume outflow.

An inter-comparison with other space-borne instruments such as TES and ACE-FTS will be helpful to interpret the difference and the biases between the retrieved HCOOH columns and thus between their respective $ER_{(HCOOH/CO)}$.

7. Data availability

The IASI FORLI CO and HCOOH products are publicly available via the Aeris data infrastructure, using the following links: http://iasi.aeris-data.fr/CO/ and http://iasi.aeris-data.fr/HCOOH/.

Acknowledgments

The IASI mission is a joint mission of EUMETSAT and the Centre National d'Etudes Spatiales (CNES, France). The IASI L1 data are distributed in near real time by EUMETSAT through the EUMETCast system distribution. We thank the MODIS team for providing public access to fire products MCD14ML and the land cover type data product MCD12Q1. This MCD14ML MODIS data set was provided by the University of Maryland and NASA FIRMS operated by NASA/GSFC/ESDIS with funding provided by NASA/HQ. The authors thank S. Whitburn (ULB) for his help on the MODIS files. They also thank J. Hadji-Lazaro (LATMOS) and L. Clarisse (ULB) for preparing the IASI ΔT_b data set. The authors also acknowledge ECMWF for free access to the meteorological data.

References

Akagi, S. K., Yokelson, R. J., Wiedinmyer, C., Alvarado, M. J., Reid, J. S., Karl, T., Crounse, J. D., and Wennberg, P. O.: Emission factors for open and domestic biomass burning for use in atmospheric models, Atmos. Chem. Phys., 11, 4039-4072, doi:10.5194/acp-11-4039-2011, 2011.

Andreae, M. O., Andreae, T. W., Talbot, R. W., and Harriss, R. C.: Formic and acetic acid over the central Amazon region, Brazil, I. Dry season, J. Geophys. Res., 93, 1616–1624, doi:10.1029/JD093iD02p01616, 1988.

Andrews, D. U., Heazlewood, B. R., Maccarone, A. T., Conroy, T., Payne, R. J., Jordan, M. J. T., and Kable, S. H.: Photo-tautomerization of acetaldehyde to vinyl alcohol: a potential route to tropospheric acids, Science, 337, 1203–1206, doi:10.1126/science.1220712, 2012.

Beirle, S., K. F. Boersma, U. Platt, M. G. Lawrence, and T. Wagner : Megacity emissions and lifetimes of nitrogen oxides probed from space, Science, 333, 1737–1739, doi:10.1126/science.1207824, 2011.

Bisht, D. S., Tiwari, S., Srivastava, A. K., Singh, J. V., Singh, B. P., Srivastava, M. K. : High concentration of acidic species in rainwater at Varanasi in the Indo-Gangetic Plains, India, Nat Hazards, 75, 2985–3003, DOI 10.1007/s11069-014-1473-0, 2014.

Bohn, B., Siese, M., and Zetzschn, C.: Kinetics of the $OH+C_2H_2$ reaction in the presence of O_2, J. Chem. Soc. Faraday T., 92, 1459–1466, 1996.

Cady-Pereira, K. E., Chaliyakunnel, S., Shephard, M. W., Millet, D. B., Luo, M., and Wells, K. C.: HCOOH measurements from space: TES retrieval algorithm and observed global distribution, Atmos. Meas. Tech., 7, 2297-2311, doi:10.5194/amt-7-2297-2014, 2014.

Chaliyakunnel, S., Millet, D. B., Wells, K. C., Cady-Pereira, K. E., and Shephard, M. W.: A Large Underestimate of Formic Acid from Tropical Fires: Constraints from Space-Borne Measurements, Environ. Sci. Technol., 50, 5631–5640, doi:10.1021/acs.est.5b06385, 2016.

Chameides, W. L. and Davis, D. D.: Aqueous-phase source of formic acid in clouds. Nature 304, 427-429, 1983.

Channan, S., Collins, K., and Emanuel, W. R.,Global mosaics of the standard MODIS land cover type data. University of Maryland and the Pacific Northwest National Laboratory, College Park, Maryland, USA, 2014.

Clerbaux, C., Boynard, A., Clarisse, L., George, M., Hadji-Lazaro, J., Herbin, H., Hurtmans, D., Pommier, M., Razavi, A., Turquety, S., Wespes, C., and Coheur, P.-F.: Monitoring of atmospheric composition using the thermal infrared IASI/MetOp sounder, Atmos. Chem. Phys., 9, 6041-6054, doi:10.5194/acp-9-6041-2009, 2009.

Clubb, A. E., Jordan, M. J. T., Kable, S. H., and Osborn, D. L.: Phototautomerization of Acetaldehyde to vinyl alcohol: a primary process in UV-irradiated acetaldehyde from 295 to 335nm, J. Phys. Chem. Lett., 3, 3522–3526, 2012.

Coheur, P.-F., Herbin, H., Clerbaux, C., Hurtmans, D., Wespes, C., Carleer, M., Turquety, S., Rinsland, C. P., Remedios, J., Hauglustaine, D., Boone, C. D., and Bernath, P. F.: ACE-FTS observation of a young biomass burning plume: first reported measurements of C_2H_4, C_3H_6O, H_2CO and PAN by infrared occultation from space, Atmos. Chem. Phys., 7, 5437-5446, doi:10.5194/acp-7-5437-2007, 2007.

Coheur, P.-F., Clarisse, L., Turquety, S., Hurtmans, D., and Clerbaux, C.: IASI measurements of reactive trace species in biomass burning plumes, Atmos. Chem. Phys., 9, 5655-5667, doi:10.5194/acp-9-5655-2009, 2009.

Crevoisier, C., Chédin, A., Matsueda, H., Machida, T., Armante, R., and Scott, N. A.: First year of upper tropospheric integrated content of CO_2 from IASI hyperspectral infrared observations, Atmos. Chem. Phys., 9, 4797-4810, doi:10.5194/acp-9-4797-2009, 2009.

Crevoisier, C., Clerbaux, C., Guidard, V., Phulpin, T., Armante, R., Barret, B., Camy-Peyret, C., Chaboureau, J.-P., Coheur, P.-F., Crépeau, L., Dufour, G., Labonnote, L., Lavanant, L., Hadji-Lazaro, J., Herbin, H., Jacquinet-Husson, N., Payan, S., Péquignot, E., Pierangelo, C., Sellitto, P., and Stubenrauch, C.: Towards IASI-New Generation (IASI-NG): impact of improved spectral resolution and radiometric noise on the retrieval of thermodynamic, chemistry and climate variables, Atmos. Meas. Tech., 7, 4367-4385, doi:10.5194/amt-7-4367-2014, 2014.

Dee, D. P., Uppala, S. M., Simmons, A. J., Berrisford, P., Poli, P., Kobayashi, S., Andrae, U., Balmaseda, M. A., Balsamo, G., Bauer, P., Bechtold, P., Beljaars, A. C. M., van de Berg, L., Bidlot, J., Bormann, N., Delsol, C., Dragani, R., Fuentes, M., Geer, A. J., Haimberger, L., Healy, S. B., Hersbach, H., Hólm, E. V., Isaksen, L., Kållberg, P., Köhler, M., Matricardi, M. , McNally, A. P., Monge-Sanz, B. M., Morcrette, J.-J., Park, B.-K., Peubey, C., de Rosnay, P., Tavolato, C., Thépaut, J.-N. and

Vitart, F.: The ERA-Interim reanalysis: configuration and performance of the data assimilation system, Quarterly Journal of the Royal Meteorological Society, 137,553-597, doi = 10.1002/qj.828, 2011.

Duflot, V., Wespes, C., Clarisse, L., Hurtmans, D., Ngadi, Y., Jones, N., Paton-Walsh, C., Hadji-Lazaro, J., Vigouroux, C., De Mazière, M., Metzger, J.-M., Mahieu, E., Servais, C., Hase, F., Schneider, M., Clerbaux, C., and Coheur, P.-F.: Acetylene (C_2H_2) and hydrogen cyanide (HCN) from IASI satellite observations: global distributions, validation, and comparison with model, Atmos. Chem. Phys., 15, 10509-10527, doi:10.5194/acp-15-10509-2015, 2015.

De Wachter, E., Barret, B., Le Flochmoën, E., Pavelin, E., Matricardi, M., Clerbaux, C., Hadji-Lazaro, J., George, M., Hurtmans, D., Coheur, P.-F., Nedelec, P., and Cammas, J. P.: Retrieval of MetOp-A/IASI CO profiles and validation with MOZAIC data, Atmos. Meas. Tech., 5, 2843-2857, doi:10.5194/amt-5-2843-2012, 2012.

Duc, H. N., Bang, H. Q., and Quang, N. X.: Modelling and prediction of air pollutant transport during the 2014 biomass burning and forest fires in peninsular Southeast Asia, Environ. Monit. Assess, 188: 106., DOI: 10.1007/s10661-016-5106-9, 2016.

Fioletov, V. E., C. A. McLinden, N. Krotkov, and C. Li : Lifetimes and emissions of SO_2 from point sources estimated from OMI, Geophys. Res. Lett., 42, 1969–1976, doi:10.1002/2015GL063148, 2015.

Friedl, M. A., Sulla-Menashe, D., Tan, B., Schneider, A., Ramankutty, N., Sibley, A. and Huang, X., MODIS Collection 5 global land cover: Algorithm refinements and characterization of new datasets, 2001-2012, Collection 5.1 IGBP Land Cover, Remote Sensing of Environment, 114 , 168–182, doi:10.1016/j.rse.2009.08.016, 2010.

Gabriel, R., Schäfer, L., Gerlach, C., Rausch, T. and Kesselmeier, J.: Factors controlling the emissions of volatile organic acids from leaves of Quercus ilex L. (Holm oak). Atmos. Env., 33, 1347-1355, 1999.

George, M., Clerbaux, C., Hurtmans, D., Turquety, S., Coheur, P.-F., Pommier, M., Hadji-Lazaro, J., Edwards, D. P., Worden, H., Luo, M., Rinsland, C., and McMillan, W.: Carbon monoxide distributions from the IASI/METOP mission: evaluation with other space-borne remote sensors, Atmos. Chem. Phys., 9, 8317-8330, doi:10.5194/acp-9-8317-2009, 2009.

Giglio, L., van der Werf, G. R., Randerson, J. T., Collatz, G. J., and Kasibhatla, P.: Global estimation of burned area using MODIS active fire observations, Atmos. Chem. Phys., 6, 957-974, doi:10.5194/acp-6-957-2006, 2006.

Giglio, L.: MODIS Collection 5 Active Fire Product User's Guide, v2.5, Updated 31 March 2013, 2013.

González Abad, G., Bernath, P. F., Boone, C. D., McLeod, S. D., Manney, G. L., and Toon, G. C.: Global distribution of upper tropospheric formic acid from the ACE-FTS, Atmos. Chem. Phys., 9, 8039-8047, doi:10.5194/acp-9-8039-2009, 2009.

Goode, J., Yokelson, R., Ward, D., Susott, R., Babbitt, R., Davies, M., and Hao, W.: Measurements of excess O_3, CO_2, CO, CH_4, C_2H_4, C_2H_2, HCN, NO, NH_3, HCOOH, CH_3COOH, HCHO, and CH_3OH in 1997 Alaskan biomass burning plumes by airborne Fourier transform infrared spectroscopy (AFTIR), J. Geophys. Res., 105, 22147, doi:10.1029/2000JD900287, 2000.

Graedel, T., and Eisner, T.: Atmospheric formic acid from formicine ants: a preliminary assessment, Tellus B, 40, 335–339, 1988.

Grosjean, D.: Organic acids in southern California air: ambient concentrations, mobile source emissions, in situ formation and removal processes, Environ. Sci. Technol., 23, 1506–1514, 1989.

Grutter, M., Glatthor, N., Stiller, G. P., Fischer, H., Grabowski, U., Höpfner, M., Kellmann, S., Linden, A., and von Clarmann, T.: Global distribution and variability of formic acid as observed by MIPAS-ENVISAT, J. Geophys. Res., 115, D10303, doi:10.1029/2009JD012980, 2010.

Hatakeyama, S., Washida, N., and Akimoto, H.: Rate constants and mechanisms for the reaction of hydroxyl (OD) radicals with acetylene, propyne, and 2-butyne in air at 297±2K, J. Phys. Chem., 6, 90, 173–178, 1986.

Hurtmans, D., Coheur, P.-F., Wespes, C., Clarisse, L., Scharf, O., Clerbaux, C., Hadji-Lazaro, J., George, M., and Turquety, S.: FORLI radiative transfer and retrieval code for IASI, J. Quant. Spectrosc. Radiat. Transf., 113, 1391–1408, doi:10.1016/j.jqsrt.2012.02.036, 2012.

Hurst, D. F., Griffith, D. W. T., and Cook, G. D.: Trace gas emissions from biomass burning in tropical Australian savannas. Journal of Geophysical Research, 99(D8), 16441–16456, doi:10.1029/94JD00670, 1994.

Jacob, D.: Chemistry of OH in remote clouds and its role in the production of formic acid and peroxymonosulfate, J. Geophys. Res., 91, 9807–9826, 1986.

Justice, C.O., Giglio, L., Korontzi, S., Owens, J., Morisette, J.T., Roy, D., Descloitres, J., Alleaume, S., Petitcolin, F., Kaufman, Y.: The MODIS fire products. Rem. Sens. Environ. 83, 244-262.2002.

Kaskaoutis, D. G., Kumar, S., Sharma, D., Singh, R. P., Kharol, S. K., Sharma, M., Singh, A. K., Singh, S., Singh, A., and Singh, D.: Effects of crop residue burning on aerosol properties, plume characteristics, and long-range transport over northern India, J. Geophys. Res. Atmos., 119, 5424–5444, doi:10.1002/2013JD021357, 2014.

Kawamura, K., Ng, L.-L., and Kaplan, I.: Determination of organic acids (C_1-C_{10}) in the atmosphere, motor exhausts, and engine oils, Environ. Sci. Technol., 19, 1082–1086, 1985.

Keene, W. and Galloway, J.: Organic acidity in precipitation of North America, Atmos. Environ., 18, 2491–2497, 1984.

Keene, W. and Galloway, J.: The biogeochemical cycling of formic and acetic acids through the troposphere: An overview of current understanding, Tellus B, 40, 322–334, 1988.

Kerzenmacher, T., Dils, B., Kumps, N., Blumenstock, T., Clerbaux, C., Coheur, P.-F., Demoulin, P., García, O., George, M., Griffith, D. W. T., Hase, F., Hadji-Lazaro, J., Hurtmans, D., Jones, N., Mahieu, E., Notholt, J., Paton-Walsh, C., Raffalski, U., Ridder, T., Schneider, M., Servais, C., and De Mazière, M.: Validation of IASI FORLI carbon monoxide retrievals using FTIR data from NDACC, Atmos. Meas. Tech., 5, 2751-2761, doi:10.5194/amt-5-2751-2012, 2012.

Krol, M., Peters, W., Hooghiemstra, P., George, M., Clerbaux, C., Hurtmans, D., McInerney, D., Sedano, F., Bergamaschi, P., El Hajj, M., Kaiser, J. W., Fisher, D., Yershov, V., and Muller, J.-P.: How much CO was emitted by the 2010 fires around Moscow?, Atmos. Chem. Phys., 13, 4737-4747, doi:10.5194/acp-13-4737-2013, 2013.

Lee, A., Goldstein, A. H., Kroll, J. H., Ng, N. L., Varutbangkul, V., Flagan, R. C., and Seinfeld, J. H.: Gas-phase products and secondary aerosol yields from the photooxidation of different terpenes, J. Geophys. Res., 111, D17305, doi: 10.1029/2006JD007050, 2006.

Neeb, P., Sauer, F., Horie, O., and Moortgat, G. K.: Formation of hydroxymethyl hydroperoxide and formic acid in alkene ozonolysis in the presence of water vapour, Atmos. Environ., 31, 1417–1423, 1997.

Ohara, T., Akimoto, H., Kurokawa, J., Horii, N., Yamaji, K., Yan, X., and Hayasaka, T.: An Asian emission inventory of anthropogenic emission sources for the period 1980–2020, Atmos. Chem. Phys., 7, 4419-4444, doi:10.5194/acp-7-4419-2007, 2007.

Ohta, K., Ogawa, H. , and Mizuno, T.: Abiological formation of formic acid on rocks in nature. Appl. Geochem. 15, 91-95, 2000.

Paris, J.-D., Ciais, P., Nedelec, P., Ramonet, M., Belan, B. D., Arshinov, M. Yu., Golitsyn, G. S., Granberg, I., Stohl, A., Cayez, G., Athier, G., Boumard, F. and Cousin, J.-M. : The YAK-AEROSIB transcontinental aircraft campaigns: new insights on the transport of CO_2, CO and O_3 across Siberia. Tellus B, 60, 551–568, doi:10.1111/j.1600-0889.2008.00369.x, 2008.

Paton-Walsh, C., Jones, N. B., Wilson, S. R., Haverd, V., Meier, A., Griffith, D. W. T., and Rinsland, C. P.: Measurements of trace gas emissions from Australian forest fires and correlations with coincident measurements of aerosol optical depth, J. Geophys. Res., 110, D24305, doi:10.1029/2005JD006202, 2005.

Paulot, F., et al..: Importance of secondary sources in the atmospheric budgets of formic and acetic acids, Atmos. Chem. Phys., 11, 1989–2013, doi:10.5194/acp-11-1989-2011, 2011.

Pochanart, P., Akimoto, H., Kajii, Y., Potemkin, V. M., and Khodzher, T. V. : Regional background ozone and carbon monoxide variations in remote Siberia/East Asia, J. Geophys. Res., 108(D1), 4028, doi:10.1029/2001JD001412, 2003.

Pommier, M., Law, K. S., Clerbaux, C., Turquety, S., Hurtmans, D., Hadji-Lazaro, J., Coheur, P.-F., Schlager, H., Ancellet, G., Paris, J.-D., Nédélec, P., Diskin, G. S., Podolske, J. R., Holloway, J. S., and Bernath, P.: IASI carbon monoxide validation over the Arctic during POLARCAT spring and summer campaigns, Atmos. Chem. Phys., 10, 10655-10678, doi:10.5194/acp-10-10655-2010, 2010.

Pommier, M., McLinden, C. A., and Deeter, M.: Relative changes in CO emissions over megacities based on observations from space, Geophys. Res. Lett., 40, 3766–3771, doi:10.1002/grl.50704, 2013.

Pommier, M., Clerbaux, C., Coheur, P.-F., Mahieu, E., Müller, J.-F., Paton-Walsh, C., Stavrakou, T., and Vigouroux, C.: HCOOH distributions from IASI for 2008–2014: comparison with ground-based FTIR measurements and a global chemistry-transport model, Atmos. Chem. Phys., 16, 8963-8981, doi:10.5194/acp-16-8963-2016, 2016.

R'Honi, Y., Clarisse, L., Clerbaux, C., Hurtmans, D., Duflot, V., Turquety, S., Ngadi, Y., and Coheur, P.-F.: Exceptional emissions of NH_3 and HCOOH in the 2010 Russian wildfires, Atmos. Chem. Phys., 13, 4171-4181, doi:10.5194/acp-13-4171-2013, 2013.

Rinsland, C. P., Boone, C. D., Bernath, P. F., Mahieu, E., Zander, R., Dufour, G., Clerbaux, C., Turquety, S., Chiou, L., McConnell, J. C., Neary, L., and Kaminski, J. W. : First space-based observations of formic acid (HCOOH): Atmospheric Chemistry Experiment austral spring 2004 and 2005 Southern Hemisphere tropical-mid-latitude upper tropospheric measurements, Geophys. Res. Lett., 33, L23804, doi:10.1029/2006GL027128, 2006.

Rinsland, C. P., Dufour, G., Boone, C. D., Bernath, P. F., Chiou, L., Coheur, P.-F., Turquety, S., and Clerbaux, C.: Satellite boreal measurements over Alaska and Canada during June–July 2004: Simultaneous measurements of upper tropospheric CO, C_2H_6, HCN, CH_3Cl, CH_4, C_2H_2, CH_3OH, HCOOH, OCS, and SF_6 mixing ratios, Global Biogeochem. Cycles, 21, GB3008, doi:10.1029/2006GB002795, 2007.

Rolph, G.D., Real-time Environmental Applications and Display sYstem (READY) Website (http://www.ready.noaa.gov). NOAA Air Resources Laboratory, College Park, MD, 2017.

Rodgers, C. D.: Inverse methods for atmospheric sounding: theory and practice, Ser. Atmos. Ocean. Planet. Phys. 2, World Sci., Hackensack, NJ, 2000.

Sanhueza, E. and Andreae, M.: Emission of formic and acetic acids from tropical savanna soils, Geophys. Res. Lett., 18, 1707–1710, 1991.

Schreier, S. F., Richter, A., Kaiser, J. W., and Burrows, J. P.: The empirical relationship between satellite-derived tropospheric NO_2 and fire radiative power and possible implications for fire emission rates of NO_x, Atmos. Chem. Phys., 14, 2447-2466, doi:10.5194/acp-14-2447-2014, 2014.

Sinha, P., P. Hobbs, V., Yokelson, R. J., Bertschi, I. T., Blake, D. R., Simpson, I. J., Gao, S., Kirchstetter, T. W., and Novakov, T.: Emissions of trace gases and particles from savanna fires in southern Africa, J. Geophys. Res., 108, 8487, doi:10.1029/2002JD002325, D13, 2003.

Sinha, P., P. Hobbs, V., Yokelson, R. J., Blake, D. R., Gao, S., and Kirchstetter, T. W.: Emissions from miombo woodland and dambo grassland savanna fires, J. Geophys. Res., 109, D11305, doi:10.1029/2004JD004521, 2004.

Srinivas, R., Beig, G., and Peshin S. K. : Role of transport in elevated CO levels over Delhi during onset phase of monsoon, Atmos. Env,140, 234-241, http://dx.doi.org/10.1016/j.atmosenv.2016.06.003, 2016.

Stavrakou, T., Müller, J-F., Peeters, J., Razavi, A., Clarisse, L., Clerbaux, C., Coheur, P.-F., Hurtmans, D., and De Mazière, M.: Satellite evidence for a large source of formic acid from boreal and tropical forests, Nat. Geosci., 5, 26–30, doi:10.1038/ngeo1354, 2012.

Tereszchuk, K. A., González Abad, G., Clerbaux, C., Hurtmans, D., Coheur, P.-F., and Bernath, P. F.: ACE-FTS measurements of trace species in the characterization of biomass burning plumes, Atmos. Chem. Phys., 11, 12169-12179, doi:10.5194/acp-11-12169-2011, 2011.

Tereszchuk, K. A., González Abad, G., Clerbaux, C., Hadji-Lazaro, J., Hurtmans, D., Coheur, P.-F., and Bernath, P. F.: ACE-FTS observations of pyrogenic trace species in boreal biomass burning plumes during BORTAS, Atmos. Chem. Phys., 13, 4529-4541, doi:10.5194/acp-13-4529-2013, 2013.

Turquety, S., Hurtmans, D., Hadji-Lazaro, J., Coheur, P.-F., Clerbaux, C., Josset, D., and Tsamalis, C.: Tracking the emission and transport of pollution from wildfires using the IASI CO retrievals: analysis of the summer 2007 Greek fires, Atmos. Chem. Phys., 9, 4897-4913, doi:10.5194/acp-9-4897-2009, 2009.

Vadrevu, K. P., Lasko, K., Giglio, L., and Justice, C.: Vegetation fires, absorbing aerosols and smoke plume characteristics in diverse biomass burning regions of Asia, Environ. Res. Lett., 10, 2371-2379, DOI:10.1039/c4em00307a, 2015.

van der Werf, G. R., Randerson, J. T., Giglio, L., Collatz, G. J., Mu, M., Kasibhatla, P. S., Morton, D. C., DeFries, R. S., Jin, Y., and van Leeuwen, T. T.: Global fire emissions and the contribution of deforestation, savanna, forest, agricultural, and peat fires (1997–2009), Atmos. Chem. Phys., 10, 11707-11735, doi:10.5194/acp-10-11707-2010, 2010.

Viatte, C., Strong, K., Hannigan, J., Nussbaumer, E., Emmons, L. K., Conway, S., Paton-Walsh, C., Hartley, J., Benmergui, J., and Lin, J.: Identifying fire plumes in the Arctic with tropospheric FTIR measurements and transport models, Atmos. Chem. Phys., 15, 2227-2246, doi:10.5194/acp-15-2227-2015, 2015.

Vigouroux, C., Stavrakou, T., Whaley, C., Dils, B., Duflot, V., Hermans, C., Kumps, N., Metzger, J.-M., Scolas, F., Vanhaelewyn, G., Müller, J.-F., Jones, D. B. A., Li, Q., and De Mazière, M.: FTIR time-series of biomass burning products (HCN, C_2H_6, C_2H_2, CH_3OH, and HCOOH) at Reunion Island (21° S, 55° E) and comparisons with model data, Atmos. Chem. Phys., 12, 10367-10385, doi:10.5194/acp-12-10367-2012, 2012.

White, F.: UNESCO/AETFAT/UNSO vegetation map of Africa, scale 1:5,000,000, UNESCO, Paris, 1981.

Whitburn, S., Van Damme, M., Kaiser, J. W., van der Werf, G. R., Turquety, S., Hurtmans, D., Clarisse, L., Clerbaux, C., and Coheur, P.-F.: Ammonia emissions in tropical biomass burning regions: Comparison between satellite-derived emissions and bottom-up fire inventories, Atmos. Environ, 121, 42–54, doi:10.1016/j.atmosenv.2015.03.015, 2015.

Whitburn, S., Van Damme, M., Clarisse, L., Hurtmans, D., Clerbaux, C., and Coheur, P.-F.: IASI-derived NH_3 enhancement ratios relative to CO for the tropical biomass burning regions, Atmos. Chem. Phys. Discuss., https://doi.org/10.5194/acp-2017-331, in review, 2017.

Wooster, M. J., Roberts, G., Perry, G. L. W., and Kaufman, Y. J.: Retrieval of biomass combustion rates and totals from fire radiative power observations: FRP derivation and calibration relationships between biomass consumption and fire radiative energy release, J. Geophys. Res., 110, D24311, doi:10.1029/2005JD006318, 2005.

Yokelson, R. J., Bertschi, I. T., Christian, T. J., Hobbs, P. V., Ward, D. E., and Hao, W. M.: Trace gas measurements in nascent, aged, and cloud-processed smoke from African savanna fires by airborne Fourier transform infrared spectroscopy (AFTIR), J. Geophys. Res., 108, 8478, doi:10.1029/2002JD002322, 2003.

Yokelson, R. J., Karl, T., Artaxo, P., Blake, D. R., Christian, T. J., Griffith, D. W. T., Guenther, A., and Hao, W. M.: The Tropical Forest and Fire Emissions Experiment: overview and airborne fire emission factor measurements, Atmos. Chem. Phys., 7, 5175-5196, doi:10.5194/acp-7-5175-2007, 2007.

Yokelson, R. J., Christian, T. J., Karl, T. G., and Guenther, A.: The tropical forest and fire emissions experiment: laboratory fire measurements and synthesis of campaign data, Atmos. Chem. Phys., 8, 3509-3527, doi:10.5194/acp-8-3509-2008, 2008.

Yokelson, R. J., Akagi, S. K., Griffith, D. W. T., and Johnson, T. J.: Interactive comment on "Exceptional emissions of NH_3 and HCOOH in the 2010 Russian wildfires" by Y. R'Honi et al., Atmos. Chem. Phys. Discuss., 12, C11864–C11868, 2013.

Table 1. Upper row: Correlation coefficients between the HCOOH total columns and the CO total columns measured by IASI for the period between 2008 and 2014 over the seven studied regions. Lower row: As upper row but with only MODIS fire hotspot having a surface wind speed lower than 1.44 m/s. Each IASI data is selected in an area of 50 km around the MODIS fire hotspot and up to 5h after the time recorded for each fire. The number of fires characterized by HCOOH and CO total columns is given in parenthesis.

	AMA	AUS	IND	SEA	SAF	NAF	SIB
r	0.78 (13342)	0.63 (1525)	0.53 (1641)	0.84 (1865)	0.78 (12227)	0.58 (21139)	0.65 (22353)
	0.79 (4580)	0.65 (93)	0.65 (340)	0.86 (528)	0.80 (895)	0.53 (1095)	0.72 (2097)

Table 2. Enhancement ratio of HCOOH relative to CO (mol/mol) with its standard deviation compared to enhancement ratios of HCOOH relative to CO and emissions ratios of HCOOH reported in the literature for the seven studied regions.

Region	**Enhancement Ratio to CO (mol/mol) – this work**	Enhancement Ratio to CO (mol/mol) found in literature	Emission Ratio to CO (mol/mol) found in literature	Instrument used
AMA	**$7.3\times10^{-3} \pm 0.08\times10^{-3}$**	$5.1\times10^{-3} \pm 1.5\times10^{-3}$ (González Abad et al., 2009)*		ACE-FTS
		$6.7\times10^{-3} \pm 2.1\times10^{-3}$ (Chaliyakunnel et al., 2016)		TES
AUS	**$11.1\times10^{-3} \pm 1.37\times10^{-3}$**	$4.5\times10^{-3} \pm 5.1\times10^{-3}$ (Chaliyakunnel et al., 2016)		TES
		$21.0\times10^{-3} \pm 10.0\times10^{-3}$ (Paton-Walsh et al., 2005)*		Ground-based FTIR
IND	**$6.8\times10^{-3} \pm 0.44\times10^{-3}$**	None		-
SEA	**$5.8\times10^{-3} \pm 0.15\times10^{-3}$**	None		-
NAF	**$4.0\times10^{-3} \pm 0.19\times10^{-3}$**	$2.8\times10^{-3} \pm 0.4\times10^{-3}$ (Chaliyakunnel et al., 2016)		TES
SAF	**$5.0\times10^{-3} \pm 0.13\times10^{-3}$**	$2.6\times10^{-3} \pm 0.3\times10^{-3}$ (Chaliyakunnel et al., 2016)		TES
		$4.6\times10^{-3} \pm 0.3\times10^{-3}$ (Vigouroux et al., 2012)		Ground-based FTIR
		5.1×10^{-3} (Coheur et al., 2007)		ACE-FTS
		$11.3\times10^{-3} \pm 7.6\times10^{-3}$ (Rinsland et al., 2006)*		ACE-FTS
			$5.9\times10^{-3} \pm 2.2\times10^{-3}$ (Yokelson et al., 2003)	Airborne FTIR
			$5.1\text{-}8.7\times10^{-3}$ (Sinha al., 2003)	Airborne FTIR
SIB	**$4.4\times10^{-3} \pm 0.09\times10^{-3}$**	$0.77\text{-}6.41\times10^{-3}$ (Tereszchuk et al., 2013)		ACE-FTS
		$2.69\text{-}15.93\times10^{-3}$ (Viatte et al., 2015)		Ground-based FTIR
		$10.0\text{-}32.0\times10^{-3}$ (R'honi et al., 2013)		IASI

* Their "emission ratios" are requalified as enhancement ratios in this study since their ratios were not measured at the origin the fire emission but at high altitudes and/or further downwind of the fires.

Table 3. Enhancement ratio of HCOOH relative to CO (mol/mol) with its standard deviation and enhancement ratio of HCOOH relative to CO (mol/mol) by biome with its standard deviation calculated in this work. For each enhancement ratio by biome, the correlation coefficient and the number of MODIS hotspots are provided. The enhancement ratios are compared to emission ratios calculated from emission factors given in the literature for the seven studied regions. For the calculation of these emission ratios, the emission factors of CO for the corresponding fuel type given in Akagi et al. (2011) are used. Emission ratios of HCOOH relative to CO (mol/mol) calculated from the emission factors of HCOOH given in Akagi et al. (2011) for the corresponding fuel type are also provided.

Region	**Enhancement Ratio to CO (mol/mol) – this work**	**Enhancement Ratio to CO (mol/mol)[1] by biome[2] – this work**	Emission Ratio to CO (mol/mol) calculated from EF_{HCOOH} given in literature and using EF_{CO} from Akagi et al. (2011)	Instrument used
AMA	**$7.3\times10^{-3} \pm 0.08\times10^{-3}$**	**$6.3\times10^{-3} \pm 0.22\times10^{-3}$ (Evergreen Broadleaf forest, r=0.81, n = 454)** **$3.0\times10^{-3} \pm 0.81\times10^{-3}$ (Open shrubland, r=0.91, n = 5)** **$7.0\times10^{-3} \pm 2.47\times10^{-3}$ (Woody savanna, r=0.63, n = 14)** **$7.6\times10^{-3} \pm 0.09\times10^{-3}$ (Savanna, r=0.79, n = 3909)** **$8.4\times10^{-3} \pm 0.39\times10^{-3}$ (Grassland, r=0.88, n = 143)** **$4.6\times10^{-3} \pm 0.35\times10^{-3}$ (Cropland, r=0.88, n = 54)**	1.8×10^{-3} – Tropical forest (Yokelson et al., 2007 ; 2008)[3] 2.7×10^{-3} – Savanna (Yokelson et al., 2007 ; 2008)[3] 2.0×10^{-3} – Savanna (Akagi et al., 2011) 5.2×10^{-3} – Tropical forest (Akagi et al., 2011)	Airborne FTIR (Yokelson et al., 2007) ; laboratory (Yokelson et al., 2008) catalogue
AUS	**$11.1\times10^{-3} \pm 1.37\times10^{-3}$**	**$5.7\times10^{-3} \pm 2.55\times10^{-3}$ (Woody savanna, r=0.6, n = 11)** **$11.2\times10^{-3} \pm 1.49\times10^{-3}$ (Savanna, r=0.65, n = 80)**	2.0×10^{-3} – Savanna (Akagi et al., 2011)	catalogue
IND	**$6.8\times10^{-3} \pm 0.44\times10^{-3}$**	**$6.6\times10^{-3} \pm 0.77\times10^{-3}$ (Woody savanna, r=0.65, n = 103)** **$6.2\times10^{-3} \pm 0.62\times10^{-3}$ (Cropland, r=0.58, n = 198)** **$8.8\times10^{-3} \pm 1.19\times10^{-3}$ (Cropland/Natural vegetation mosaic, r=0.85, n =23)**	2.0×10^{-3} – Savanna (Akagi et al., 2011) 2.7×10^{-3} – Extratropical forest (Akagi et al., 2011) 6.0×10^{-3} – Cropland (Akagi et al., 2011)	catalogue
SEA	**$5.8\times10^{-3} \pm 0.15\times10^{-3}$**	**$5.6\times10^{-3} \pm 0.20\times10^{-3}$ (Evergreen Broadleaf forest, r=0.83, n = 334)** **$6.3\times10^{-3} \pm 0.66\times10^{-3}$ (Mixed forest, r=0.76, n = 70)** **$6.2\times10^{-3} \pm 0.38\times10^{-3}$ (Woody savanna, r=0.86, n = 99)**	2.0×10^{-3} – Savanna (Akagi et al., 2011) 2.7×10^{-3} – Extratropical forest (Akagi et al., 2011) 6.0×10^{-3} – Cropland (Akagi et al., 2011)	catalogue

		$7.1\times10^{-3} \pm 0.99\times10^{-3}$ (Cropland/Natural vegetation mosaic, r=0.84, n =23)		
NAF	**$4.0\times10^{-3} \pm 0.19\times10^{-3}$**	**$3.4\times10^{-3} \pm 0.63\times10^{-3}$ (Evergreen Broadleaf forest, r=0.52, n = 78)** **$3.3\times10^{-3} \pm 0.28\times10^{-3}$ (Woody savanna, r=0.44, n = 569)** **$4.4\times10^{-3} \pm 0.29\times10^{-3}$ (Savanna, r=0.59, n = 441)** **$22.6\times10^{-3} \pm 11.06\times10^{-3}$ (Cropland/Natural vegetation mosaic, r=0.67, n = 7)**	2.0×10^{-3} – Savanna (Akagi et al., 2011)	catalogue
SAF	**$5.0\times10^{-3} \pm 0.13\times10^{-3}$**	**all hotspots are woody savanna**	3.3×10^{-3} – Tropical forest (Sinha et al., 2004)[4] 4.8×10^{-3} – Savanna (Sinha et al., 2004)[4] 4.1×10^{-3} – Tropical forest (Yokelson et al., 2003) 6.0×10^{-3} – Savanna (Yokelson et al., 2003) 13×10^{-3} – Tropical forest (Rinsland et al., 2006) 19.2×10^{-3} – Savanna (Rinsland et al., 2006) 2.0×10^{-3} – Savanna (Akagi et al., 2011) 5.2×10^{-3} – Tropical forest (Akagi et al., 2011)	Airborne FTIR Airborne FTIR ACE-FTS catalogue
SIB	**$4.4\times10^{-3} \pm 0.09\times10^{-3}$**	**$4.0\times10^{-3} \pm 0.31\times10^{-3}$ (Evergreen Needleaf forest, r=0.63, n = 245)** **$3.6\times10^{-3} \pm 0.16\times10^{-3}$ (Deciduous Needleaf forest, r=0.66, n = 659)** **$3.4\times10^{-3} \pm 0.18\times10^{-3}$ (Mixed forest, r=0.57, n = 759)** **$6.6\times10^{-3} \pm 0.48\times10^{-3}$ (Open shrubland, r=0.76, n = 143)** **$6.0\times10^{-3} \pm 0.41\times10^{-3}$ (Woody savanna, r=0.76, n = 155)** **$3.8\times10^{-3} \pm 0.65\times10^{-3}$ (Permanent wetland, r=0.6, n = 63)**	2.7×10^{-3} – Boreal forest (Akagi et al., 2011)	catalogue

[1] Only the enhancement ratio to CO calculated from a scatterplot with a correlation coefficient higher than 0.4 are reported.
[2] The type of vegetation is defined by the land cover type data product (MCD12Q1).

[3] The EF_{HCOOH} were corrected based on the comment from Yokelson et al. (2013) (EF_{HCOOH} used: 0.281 for Yokelson et al. (2007); 0.2767 for Yokelson et al. (2008)).
[4] The mean of both EF_{HCOOH} values provided in Sinha et al. (2004) were used for our $EmR_{HCOOH/CO}$ calculation

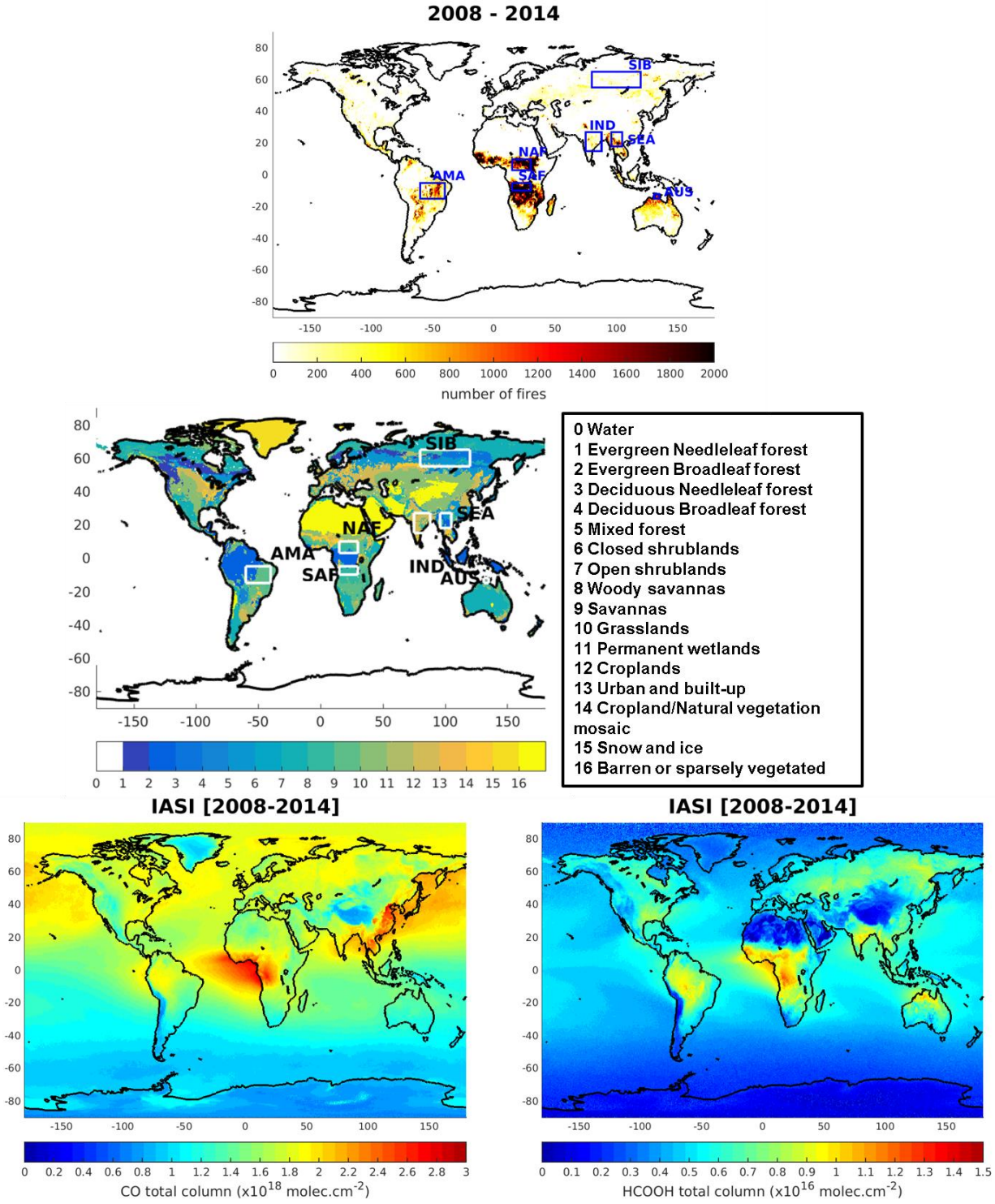

Figure 1: Top: Number of MODIS fire hotspots with a confidence percentage higher or equal to 80%, averaged on a 0.5°×0.5° grid, for the period between 2008 and 2014. The blue boxes are the regions studied in this work. Middle: Classification of the land cover type from MODIS on the same grid and highlighting the studied regions in white. Each number corresponds to the type of vegetation. Only the data between 64°S and 84°N are available. Bottom: The IASI CO total column distribution (left) and the IASI HCOOH total column distribution (right), averaged between 2008 and 2014 and on the same grid.

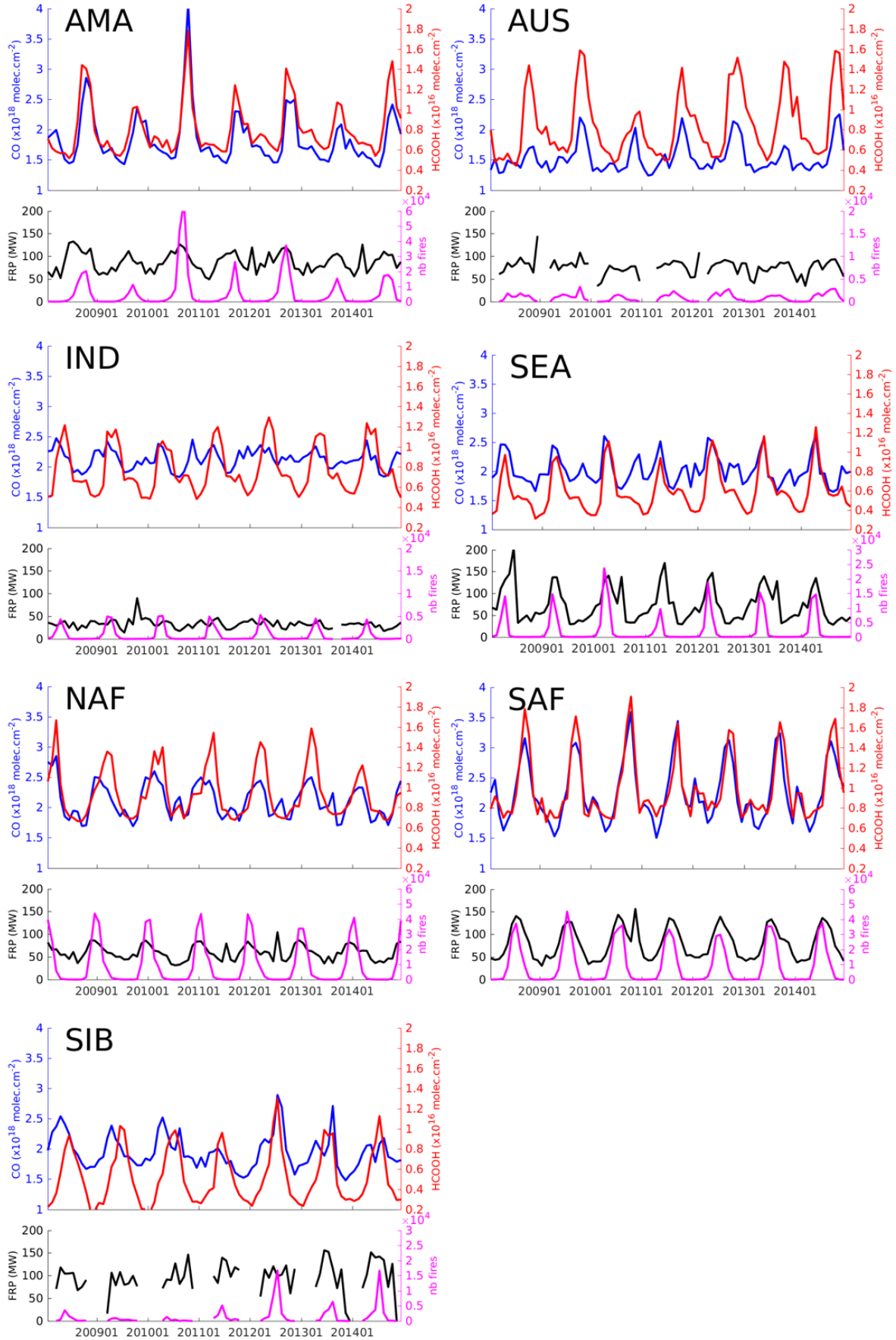

Figure 2: Time-series from 2008 to 2014 of the monthly means of IASI CO (blue) and HCOOH (red) total columns in 10^{18} molec/cm^2 and in 10^{16} molec/cm^2, respectively, FRP (black) in MegaWatts and the number of fires (magenta) from MODIS over the seven regions (AMA=Amazonia, AUS=Australia, IND = India, SEA = Southern East Asia, NAF= Northern Africa, SAF= Southern Africa, SIB= Siberia).

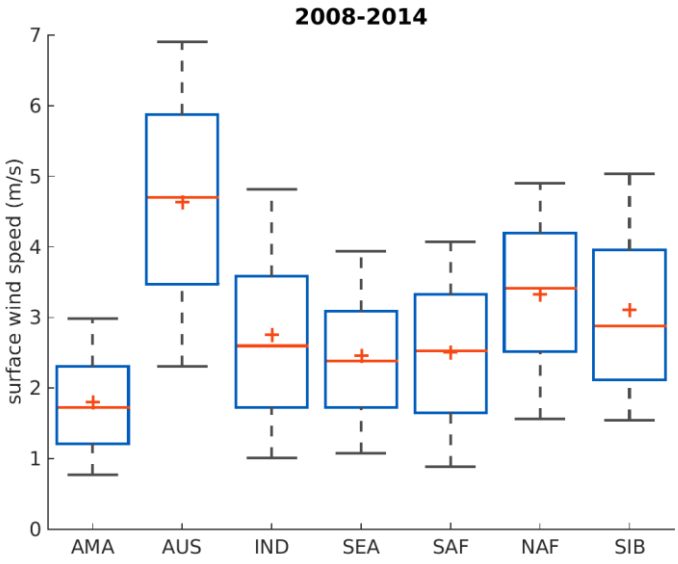

Figure 3: Box and whisker plots showing mean (red central cross), median (red central line), and 25th and 75th percentile (blue box edges) of surface wind speed for each MODIS hotspot over the studied regions (AMA=Amazonia, AUS=Australia, IND = India, SEA = Southern East Asia, NAF= Northern Africa, SAF= Southern Africa, SIB= Siberia). The whiskers encompass values from 25th-1.5×(75th-25th) to the 75th+1.5× (75th-25th). This range of values corresponds to approximately 99.3% coverage if the data are normally distributed.

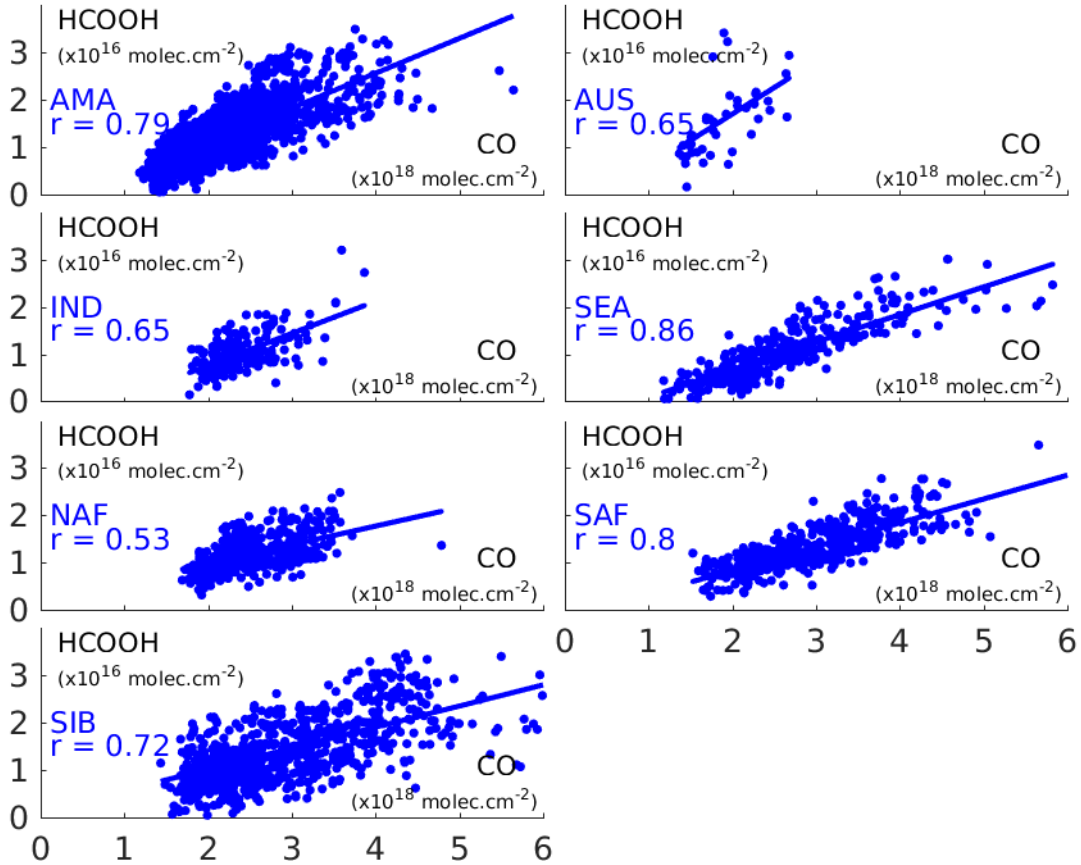

Figure 4: Scatterplots between the IASI fire-affected HCOOH total columns (in 10^{16} molec/cm^2) and the CO total columns (in 10^{18} molec/cm^2) over the seven regions (AMA=Amazonia, AUS=Australia, IND = India, SEA = Southern East Asia, NAF= Northern Africa, SAF= Southern Africa, SIB= Siberia). The linear regression is represented by the blue line and the correlation coefficient is also provided for each region.